Design, Synthesis and Thermal Analysis of Group 11 and 13 ALD Precursors

by

Amanda Kenney

A thesis submitted to the Faculty of Graduate Studies and Research in partial fulfillment of the requirements of the degree of

Master of Science

Ottawa, Ontario, K1S 5B6
Canada

September 25th, 2007

Your file Votre référence
ISBN: 978-0-494-33702-8
Our file Notre référence
ISBN: 978-0-494-33702-8

Abstract

The insertion of carbodiimides into group 13 metal-amide bonds is a facile way to synthesize homoleptic, six-coordinate guanidinato complexes of aluminum and gallium, as well as to make mixed guanidinato-amido compounds for these metals. $[Me_2NC(N^iPr)_2]_nM(NMe_2)_{3-n}$ (n = 1,2,3; M = Al, Ga) were synthesized and characterized.

All complexes are structurally characterized, and some are shown to exhibit structural features within the chelate rings and for the non-coordinated N centre, which suggests a zwitterionic resonance structure. These complexes show promise as ALD precursors; however, the decomposition route via carbodiimide deinsertion may be problematic. Since the monoguanidinato compounds avoid this decomposition route, they are the most promising as ALD precursors.

The synthesis for both the aluminum and copper ipip complexes were facile and quick and gave high yields. The new ipip ligand shows promise as a substitute for guanidinate-type ligands as it avoids the carbodiimide decomposition route. Unfortunately, the ipip complexes formed so far have been dimers, and are therefore less favourable for ALD because of their low volatility.

Acknowledgments

I would like to thank Dr. Seán Barry for all the advice and guidance during the supervision of this project and the rest of the Barry Lab (past and present) for help and advice with the synthetic and thermolysis work; and for their stimulating discussions. I would also like to thank Mom, Ira and Brad for their continued support through both the research and writing.

I would like to thank the Ontario government (OGS) for financial support. The 400 MHz NMRs were performed by Keith Borque. MS Analysis was performed by Clem Kazakoff at the University of Ottawa. The crystal structures were solved by Dr. Glenn Yap and Kevin Kreisel at the University of Delaware.

Table of Contents

Table of Figures

1 Introduction

1.1 Thin Film Deposition Methods

The future of the microelectronics industry relies on the ability to construct smaller, more compact versions of microelectronic features such as MOSFETs and magnetic memory cells. This would allow for more computational power and storage capacity on a given area and require less power, since more features would be arranged into a smaller physical space.[1] Many current research efforts focus on the development of thinner layers of conducting, semiconducting and non-conducting (dielectric) layers. Chemical deposition methods have become popular due to their high reproducibility with respect to composition and thickness control, when compared to physical deposition techniques such as sputtering.[2] In physical vapour deposition (PVD) methods, the surface is typically bombarded with a plasma that distributes material in a relatively non-uniform fashion.[3] In chemical vapour deposition (CVD) methods, chemisorption and chemical reaction drives film deposition. Atomic layer deposition (ALD) is a modification of CVD wherein two chemical reactions are separated in time by introducing reactants in a sequential cycle.[4] This allows greater thickness control by permitting one monolayer of target material to deposit per cycle.[2]

1.1.1 Atomic Layer Deposition

ALD is a sequential process in which a surface reaction is broken down into two separate steps. A typical example is the reaction of trimethyl aluminum ($Al(CH_3)_3$, TMA) and water:[5]

$$Al(CH_3)_3 + SiOH^* \rightarrow Si\text{-}O\text{-}Al(CH_3)_2^* + CH_4$$

$$Si\text{-}O\text{-}Al(CH_3)_2^* + 2\ H_2O \rightarrow Si\text{-}O\text{-}Al(OH)_2^* + 2\ CH_4$$

{*denotes a surface species}

The reaction occurs in a vacuum environment, and both precursors are introduced into this chamber in the vapour phase. As shown in Figure 1, the first step involves the introduction of the first vaporous precursor (TMA) into the reaction chamber. This reacts with a silicon surface hydroxyl group. The excess precursor and the volatile side products (here, methane gas) are removed from the reaction chamber either by evacuation or by a purge with nitrogen gas.

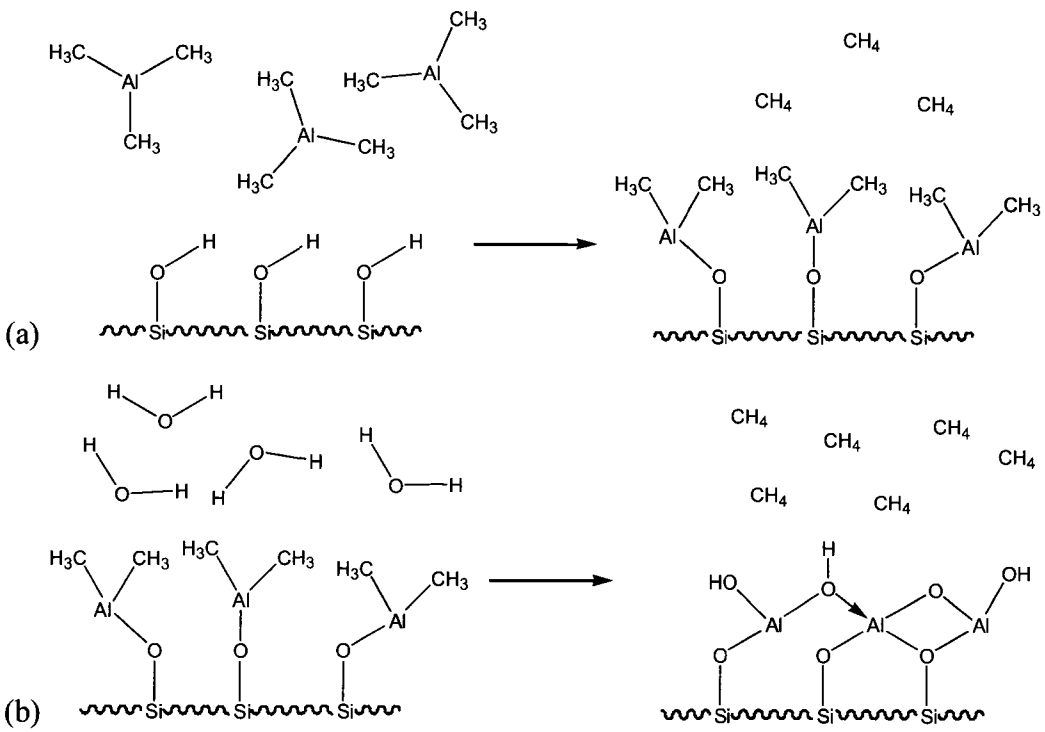

Figure 1: *Reaction of TMA and water with silicon surface to form alumina. (a) shows the reaction of TMA with silicon surface, and (b) shows the reaction of water with chemisorbed TMA.*

The second step involves entraining the second vaporous precursor (water vapour) into the reaction chamber. This reacts with the remaining methyl ligands on the aluminum, again forming methane. This process is repeated many times until the desired thickness of aluminum oxide is grown.[6]

The second reactant need not be water; this reactant commonly carries the non-metal component of the target film.[7] For example, gallium arsenide has been deposited using trimethyl gallium and arsine as sequential reactants.[6]

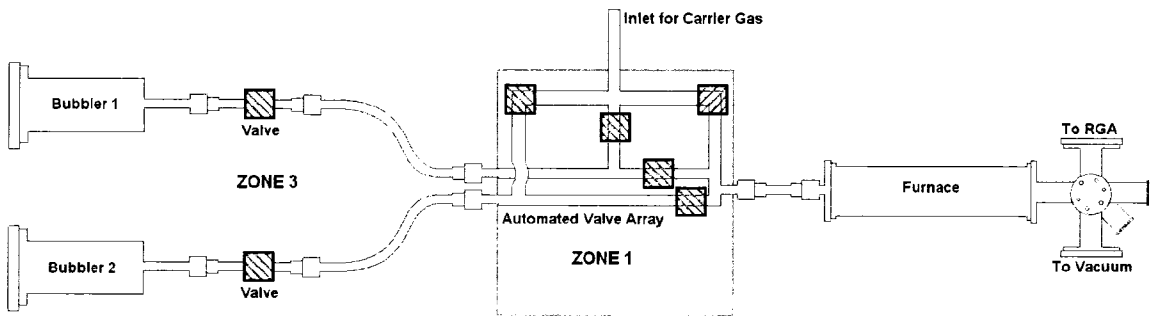

Figure 2: *Schematic of an ALD reactor.*

1.2 Ligand design

For a compound to be a successful precursor for ALD, it must possess certain factors:

1. It must be volatile.
2. It must be thermally stable.
3. It must be chemically reactive with surface groups.
4. It must produce volatile, non-reactive side products.
5. It must react to form a self-limiting monolayer.

The precursor must be volatile enough to be entrained into the reaction chamber. This can be accomplished by designing low molecular weight compounds with low melting points. Introducing branching in the structure of the ligand system can lower the melting point of a compound. This frustrates the crystallization resulting in the lowered melting point.

For typical ALD processes, it is preferable to have a liquid precursor. With solid precursors, the surface area decreases during the experiment, causing an unreliable vapour pressure. As is shown in

Figure **3**, the concentration of the precursor quickly drops off until it is shaken in the bubbler to refresh the surface area, however, this effect only lasts for a short time until the vapour concentration drops off again. With a liquid precursor, the surface area for volatilization will then be constant throughout the experiment. This allows for a reproducible vapour pressure.[8] With any vapour deposition method, it is important to have a reproducible vapour pressure since the amount of precursor in the chamber will affect the rate of deposition.

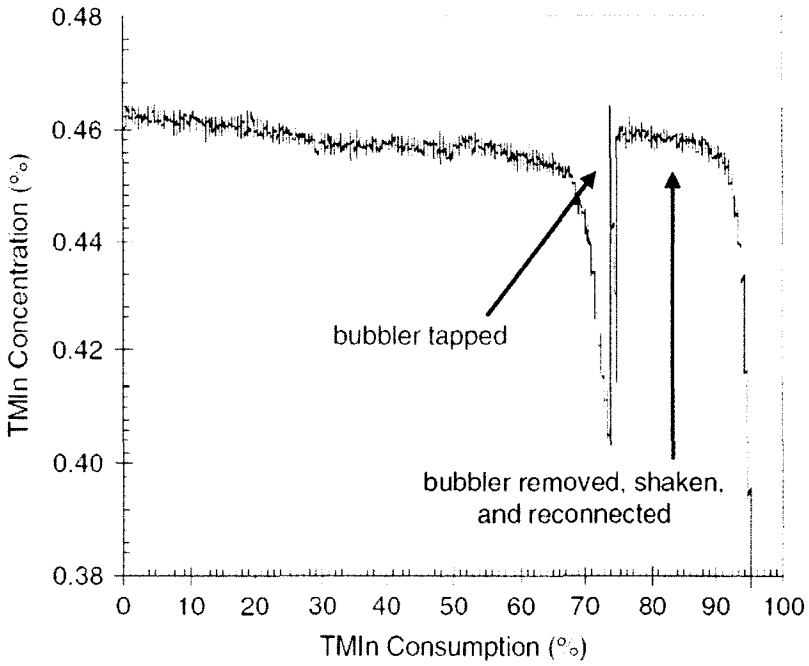

Figure 3: *Trimethyl indium (TMIn) concentration in carrier gas versus TMIn consumption at source.*[8]

The precursor must be thermally stable because it can be held at an elevated temperature to increase its vapour pressure. This can be as high as 100°C for the entire experiment, which can run for several hours. The higher temperature allows for increased volatility of precursors, and also allows low-melting point solids to be used as liquid precursors.

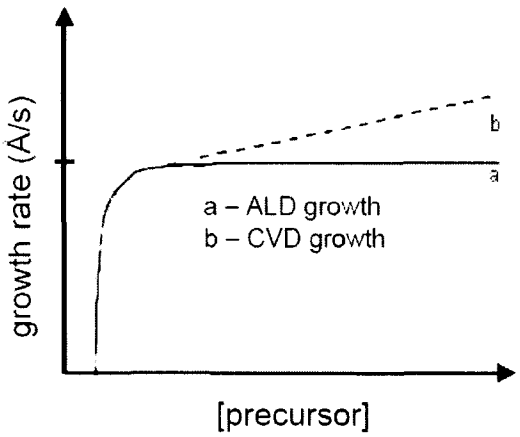

Figure 4: *ALD versus CVD growth rates. A) denotes a plateaued growth rate where the self-limiting monolayer has formed. B) shows an increasing growth rate with precursor concentration, thus indicating continual growth.*

Additionally, the precursor should not decompose at the temperature of the reaction chamber (200°C – 400°C) for similar reasons. A precursor that thermally decomposes in the deposition chamber will undergo continual, CVD-type growth. If the precursor undergoes thermal decomposition, the fragments will likely have a different reactivity with surface than the precursor as a whole. This could cause more than one layer of precursor to react with the substrate per cycle. However, for every precursor that exhibits CVD-type growth, there is an "ALD window" which occurs at a cooler temperature, before the CVD growth occurs. Additionally, the precursors should not be so stable that they do not react with the substrate. They should have a high reactivity with the substrate surface and with the second reactant gas.

The reaction of the precursor with the second reactant gas should produce volatile, non-reactive side products. If the side product can react with the chemisorbed precursor or growing target film, it could cause impurities or additional CVD-type growth.

The precursor should also react to form a self-limiting monolayer. Ideally, the precursor will react with all available surface sites, but will not react with itself, thus forming a monolayer. If the precursor thermally decomposes during the process, there is a chance that the products of the decomposition would react with the newly formed monolayer, creating another layer on top. This leads to non-uniform thickness or continual (CVD-type) growth.

One method of creating volatile precursors is to incorporate bidentate chelating ligands. These tend to produce mononuclear, low molecular weight species because the metal centre is coordinatively saturated. Guanidinate ligands are useful for this purpose. A guanidinate ligand is a bidentate ligand that bonds through two nitrogen atoms. The central carbon bonded to the coordinating nitrogens is also bonded to an exocyclic nitrogen group. Figure 5 shows an example of monoanionic and dianionic guanidinate ligands.

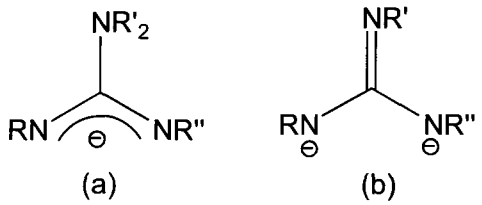

Figure 5: *Diagrams of a) a monoanionic and b) a dianionic guanidinate.*

Note that one of the differences between the mono and dianionic guanidinates is that the monoanionic guanidinate is a tetra-substituted guanidine derivative; in contrast to the dianionic guanidinate is a tri-substituted guanidine derivative.

Monoanionic Guanidinates

In the case of the monoanionic guanidinate, the metal centre is stabilized by a delocalized π-system. This delocalization allows for a second resonance structure, which makes the ligand more basic. The increased basicity allows for better stabilization of higher oxidation states in a metal.[9] Monoanionic guanidinates can be synthesized by salt metathesis,[10] insertion of a carbodiimide (R'NCNR") into a metal-nitrogen bond,[11] or by ligand exchange.[12]

Salt metathesis typically involves forming the monoanionic guanidinato lithium species by insertion at a lithium nitrogen bond, followed by a salt metathesis of the ligand with the metal chloride to form lithium chloride (Figure 6).

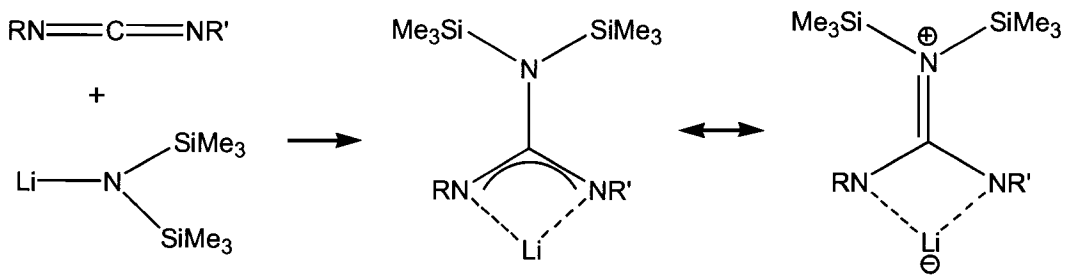

Figure 6: *Guanidinate synthesis by carbodiimide insertion into a lithium-nitrogen bond. Note that this starting material can be used in salt metathesis reactions with metal halides, and the elimination product will be lithium halide.*

Another route employing salt metathesis is the formation of the monoanionic lithium species by deprotonating a guanidine with an alkyl lithium reagent (e.g. MeLi, ^{n}BuLi), forming the guanidinato lithium and an alkane (such as methane or butane) (Figure 7).[11]

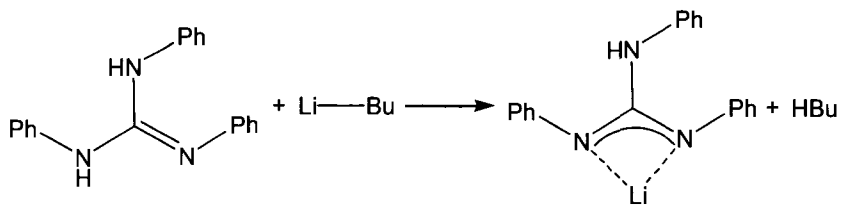

Figure 7: *Second method of lithium guanidinate synthesis to be used in a salt metathesis reaction with a metal halide.*

Salt metathesis is a very common inorganic synthetic technique that is used often in the formation of metal amidinates and guanidinates. However, it is not necessarily the most facile method. For example, aluminum compounds with these types of ligands are formed under less strident conditions and in higher yields by a carbodiimide insertion (Figure 8).[13]

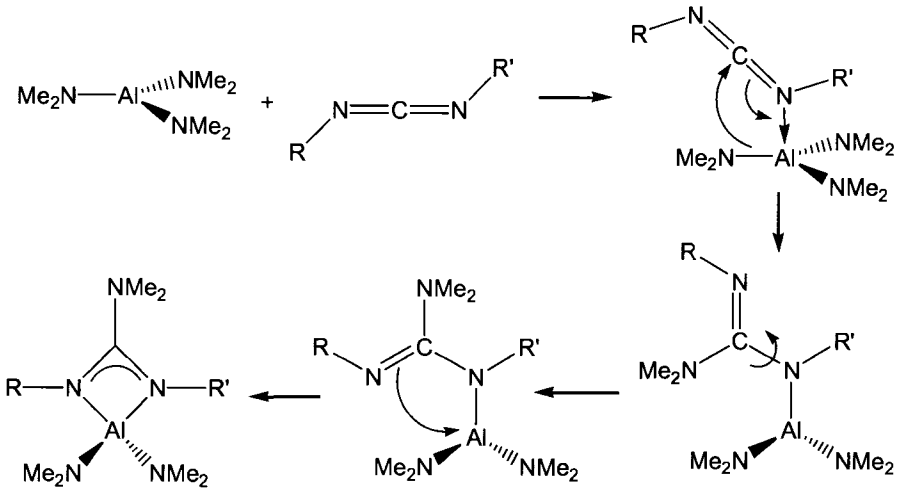

Figure 8: *Mechanism for the insertion of carbodiimide into an aluminum amide bond.*

Synthesis by carbodiimide insertion is generally quicker and easier than salt metathesis and often proceeds with higher yields.[12] This method involves the reaction of carbodiimide directly with a metal amide. There are many examples of these reactions in the literature.[12,14,15] An interesting feature of CDI insertion is that it appears to occur very quickly. For example, previous work by our group has shown that attempts to make

monoguanidinato aluminum diamide by CDI insertion resulted in bisguanidinato formation.

A third method of forming a guanidinate species is through ligand exchange.[12] The process of ligand exchange can be used to synthesize mixed ligand systems that are difficult to achieve by the previously stated methods. In ligand exchange, a pre-existing guanidinate species is required to transfer a guanidinate ligand to another species by the formation of a doubly bridged intermediate in exchange for a monodentate ligand, as shown in Figure 9, which was recently published in the 2007 Master's thesis of Allison Brazeau, from our research group.[16,17] Several recent examples of bridging guanidinate ligands have been reported.[9,15]

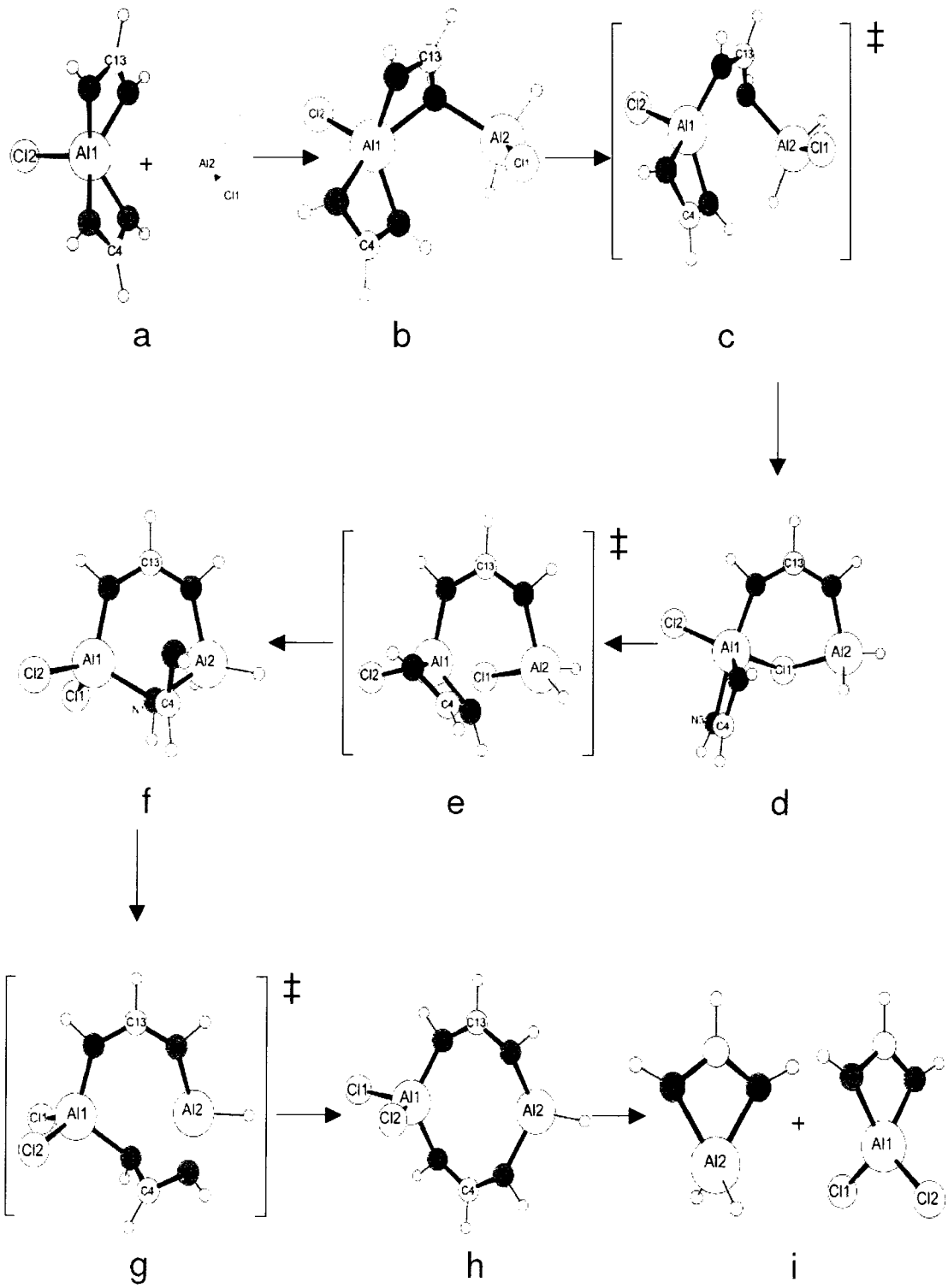

Figure 9: *Calculated mechanism of ligand exchange.*[17]

1.3 Dianionic Guanidinates

Early studies of dianionic guanidinates were actually attempts to make an η^3-coordinated species. It was thought that a dianionic guanidinate could bond in a similar fashion to trimethylmethane ligand (Figure 10). These attempts were unsuccessful since only η^2-corrdination was observed.[18,19,20]

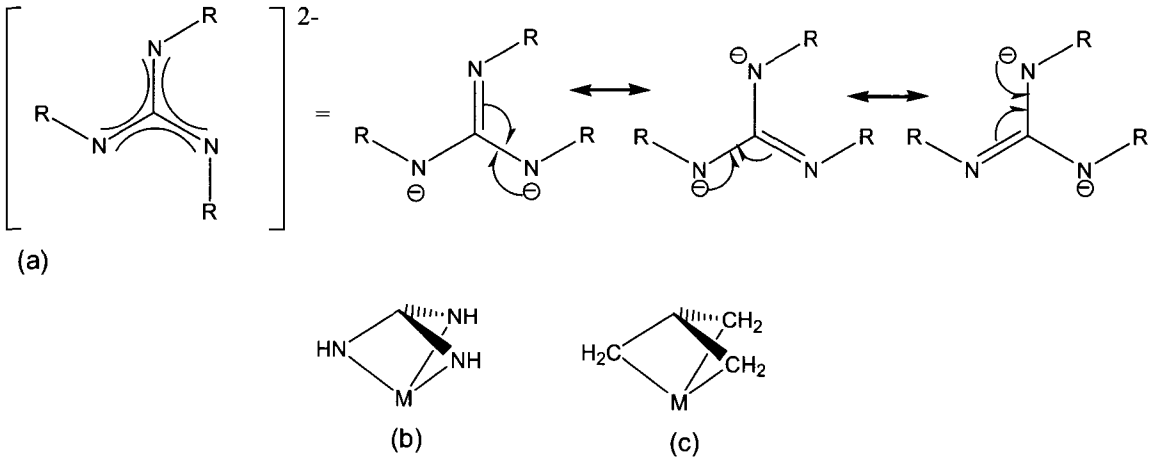

Figure 10: *(a) Resonance structures of the dianionic guanidinate.[21] Potential η3-coordination geometry of (b) a guanidinate compared to (c) the known coordination of trimethyl methane.*[21,22]

Recent efforts to make dianionic guanidinate ligands have involved the elimination of an amine group (Figure 11).[23] In this reaction, the trisubstituted guanidine is reacted with the pentakis (dimethylamido) tantalum forming the product and eliminating two equivalents of dimethylamine.

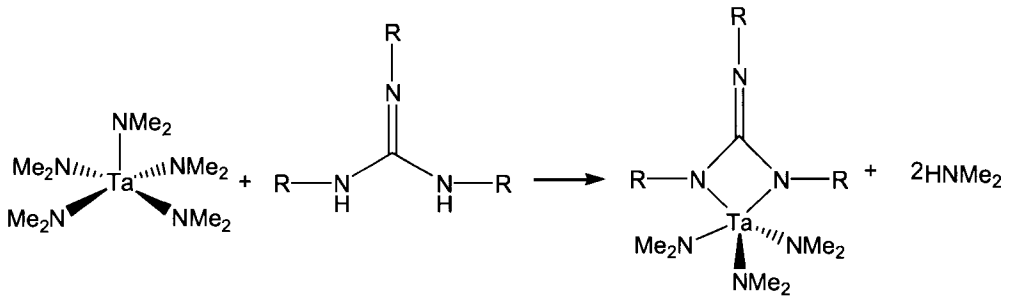

Figure 11: *Synthesis of a dianionic guanidinate ligand.*

This can also be done through a salt metathesis reaction. In the salt metathesis reaction shown below, the trisubstituted guanidine is deprotonated with two equivalents of butyl lithium (Figure 12). This forms the dianionic ligand, which can then react with a metal chloride.

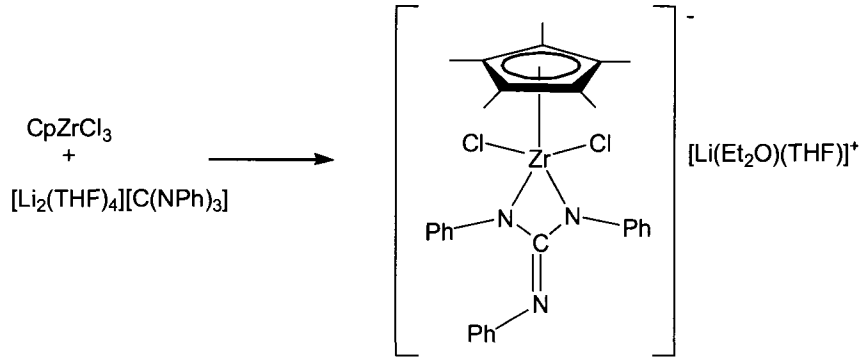

Figure 12: *Synthesis of a dianionic guanidinate by salt metathesis.*[21]

In the above case (Figure 12), an anionic zirconium complex is formed, stabilized by lithium coordinated by a solvent ligand environment. It is an interesting case of the formation of a complex of a lithium cation coordinating with solvent and the complex serving as the anion by not eliminating its halide group. This implies that salt metathesis may be a problematic route of synthesis for these types of compounds.

The monoanionic guanidinate is easier to synthesize than the dianionic guanidinate, however it may not be as thermally stable. The dianionic guanidinate allows

no deinsertion pathway for carbodiimide for metals that will not support an imide ligand, which should make it more robust to thermolysis (Figure 13).

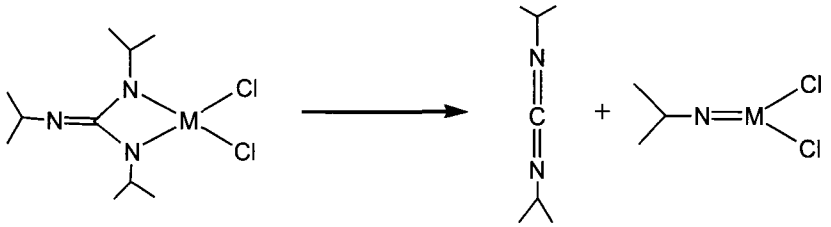

Figure 13: *Deinsertion from a dianionic guanidinate.*

1.4 Thermolysis (TGA, DSC)

Thermogravimetric analysis (TGA) and differential scanning calorimetry (DSC) are methods used to examine the thermal behaviour of a given material. TGA is based on continually weighing the material while it is being heated. This allows for determination of various thermal processes like volatility and thermal decomposition. In DSC, the temperature of the material is increased at a certain rate, and the amount of heat needed to keep that rate of temperature increase constant is measured relative to a standard. This will highlight any endo- or exothermic processes such as melting or boiling points. Knowing the likelihood and temperatures of possible decomposition can give an idea of the range of the ALD window. Also, knowing the melting and boiling points can allow for determination of the ideal temperature to hold the bubbler.

1.5 Exposure Experiments

Exposure experiments are performed to see if the precursor will form an initial monolayer with the substrate. Usually, a high-surface area sample of the substrate is used (i.e. silica powder instead of a wafer of silicon with a native oxide layer) to allow for more surface sites to be available for reaction with the precursor. The precursor is

exposed to the substrate for many hours to allow for saturation of this large surface area. The resulting monolayer-terminated surface can be characterized by different methods, including FT-IR and solid-state NMR. The temperature at which the precursor begins to react with the substrate is important since no deposition can occur below this temperature. Therefore, exposure experiments will allow the determination of the low-end of the ALD window. Together with the information derived from TGA and DSC, the range of the ALD window can be determined.

2 Group 13 Compounds

Group 13 amidinate and guanidinate complexes are novel catalysts and potential gaseous precursors to technologically important materials.[24,25] In particular, these compounds can act as precursors to group 13 nitrides, which are a family of direct band gap semiconductors, as well as precursors to thin metal films in the case of aluminum. Mixed aluminum/gallium nitrides have been applied as tunable band gap materials in high-frequency LEDs and diode lasers.[26] Monoanionic, N-substituted guanidinate anions $[RNC(NR'_2)NR]^-$ should be useful ligands for designing monomeric, volatile precursors of group 13 metals. Although previously ignored, the reversibility of this insertion mechanism is of interest as a potential thermal decomposition route. Such a deinsertion reaction provides an accessible transformation pathway for chemical vapour deposition source molecules that possess guanidinate ligands. In addition, multiple insertions of carbodiimides at a single metal centre to form bis- and tris (guanidinato) species of aluminum and gallium could lead to more stable, coordinatively saturated compounds. The synthetic mechanism and thermal reactivity require more scrutiny in this family of compounds, and so this thesis will report the synthesis and structural characterization of

novel mixed amido-guanidinato compounds of aluminum and gallium, $[Me_2NC(N^iPr)_2]_nM(NMe_2)_{3-n}$ (n = 1, 2, 3), prepared via the insertion of diisopropylcarbodiimide into the metal amido bonds of $M_2(NMe_2)_6$ (M = Al, Ga).

2.1 Synthesis

General Procedures. All manipulations were performed in a nitrogen-filled drybox. Aluminum chloride, gallium chloride, lithium dimethylamine, 1,3-diisopropyl carbodiimide, anhydrous hexane, and deuterated benzene were purchased from Aldrich Chemical Co. and used as received. The synthesis of $M_2(NMe_2)_6$ (M = Al, Ga) followed literature procedures.[27] The ^1H and ^{13}C NMR were collected on a Varian Gemini-200 or a Bruker 400 MHz spectrometer using the residual protons in the deuterated solvent for reference.

2.1.1 Aluminum monoguanidinate diamide

$[Me_2NC(N^iPr)_2]Al(NMe_2)_2$ (Compound 1). In a 50 mL flask, $Al_2(NMe_2)_6$ (1.00 g, 3.14 mmol) was dissolved in 20 mL of hexane. Diisopropylcarbodiimide (0.79 g, 6.28 mmol) was diluted in about 1 mL of toluene and then added dropwise to the solution, and the reaction mixture was stirred at room temperature overnight. The volatiles were removed in vacuo, leaving a thick liquid with a slightly yellow colour. Compound 1 was crystallized from this mixture at -30°C as a colourless, microcrystalline solid (1.675 g, 94% yield). mp 60°C. ^1H NMR (400 MHz, C_6D_6): δ 3.20 [sept, 2H, C*H*Me_2], 3.00 [s, 12H, AlN(C*H*$_3$)$_2$], 2.25 [s, 6H, CN(C*H*$_3$)$_2$], 1.05 [d, 12H, CH(C*H*$_3$)$_2$]. 13C NMR (C_6D_6): δ 169.0 [*C*N_3], 45.1 [*C*HMe_2], 41.2 [AlN(*C*H$_3$)$_2$], 38.6 [(*C*H$_3$)$_2$N], 24.4 [CH(*C*H$_3$)$_2$]. Mass

spectra *m/e* (relative abundance): 285 (23.5) M+. Anal. Calcd for $C_{13}H_{32}AlN_5$: C, 54.71; H, 11.30; N, 24.54. Found: C, 54.41; H, 11.18; N, 24.45.

2.1.2 Aluminum bisguanidinate monoamide

$[Me_2NC(N^iPr)_2]_2AlNMe_2$ (2). In a 50 mL flask, $Al_2(NMe_2)_6$ (1.16 g, 3.64 mmol) was dissolved in 20 mL of hexane. The dropwise addition of diisopropylcarbodiimide (1.839 g, 14.57 mmol) to this solution resulted in a clear, slightly yellow solution, which was stirred overnight. The volatiles were removed in vacuo, leaving a slightly yellow coloured microcrystalline powder (2.675 g, 89% crude yield). Further purification was needed because ^1H NMR indicated the presence of a small amount of compound **3**. The solid was dissolved in toluene and left to recrystallize by slow evaporation of the solvent at -30°C. Compound **2** was collected as clear, colourless crystals (2.52 g, 84% yield). mp 70°C. ^1H NMR (400 MHz, C_6D_6): δ 3.51 [sept, 4H, C*H*Me_2], 2.87 [s, 6H, AlN(C*H*$_3)_2$], 2.46 [s, 12H, CN(C*H*$_3)_2$], 1.35 [br, 12H, CH(C*H*$_3)_2$], 1.27 [br, 12H, CH(C*H*$_3)_2$]. ^{13}C NMR (400 MHz, C_6D_6): δ 170.22 [N*C*NMe_2], 45.68 [N*C*HMe_2], 41.81 [AlN(*C*H$_3)_2$], 39.33 CN(*C*H$_3)_2$], 24.57 [CH(*C*H$_3)_2$]. Mass spectra *m/e* (relative abundance): 411 (0.1) M+. Anal. Calcd for $C_{20}H_{46}AlN_7$: C, 58.36; H, 11.26; N, 23.82. Found: C, 58.08; H, 11.02; N, 23.83.

2.1.3 Aluminum trisguanidinate

$[Me_2NC(N^iPr)_2]_3Al$ (3). In a 50 mL flask, $Al_2(NMe_2)_6$ (3.00 g, 9.42 mmol) was dissolved in 25 mL of hexane. Diisopropylcarbodiimide (7.134 g, 56.53 mmol) was diluted in 15 mL of hexane and added dropwise to the solution, resulting in a translucent, slightly yellow solution. The reaction mixture was allowed to stir at room temperature, and a

white precipitate formed during this process. Colourless microcrystalline **3** was collected by filtration. The remaining solution was cooled to -30°C, and further **3** was precipitated and collected by filtration (combined yield: 8.69 g, 86% yield). mp 193°C. ^{1}H NMR (200 MHz, C_6D_6): δ 3.67 [sept, 6H, C*H*Me$_2$], 2.66 [s, 18H, CN(C*H*$_3$)$_2$], 1.46 [d, 18H, CH(C*H*$_3$)$_2$], 1.37 [d, 18H, CH(C*H*$_3$)$_2$]. ^{13}C NMR (400 MHz, C_6D_6): δ 167.9 [N*C*NMe$_2$], 45.8 [N*C*HMe$_2$], 39.9 [CN(*C*H$_3$)$_2$], 26.3 [CH(*C*H$_3$)$_2$], 24.3 [CH(*C*H$_3$)$_2$]. Mass spectra *m/e* (relative abundance): 538 (0.1) M+. Anal. Calcd for $C_{27}H_{60}AlN_9$: C, 60.30; H, 11.24; N, 23.44. Found: C, 59.98; H, 11.21; N, 23.14.

2.1.4 Gallium monoguanidinate diamide

[Me$_2$NC(N^{i}Pr)$_2$]Ga(NMe$_2$)$_2$ (4). In a 50 mL flask, $Ga_2(NMe_2)_6$ (3.00 g, 7.43 mmol) was dissolved in 20 mL of hexane. Diisopropylcarbodiimide (1.875 g, 14.86 mmol) was diluted in about 2 mL of hexane and then added dropwise to the solution. The reaction mixture was allowed to stir at room temperature for 2 days. The volatiles were removed in vacuo, leaving a viscous liquid with a slightly yellow colour. Compound **4** was crystallized from hexane at -30°C as a slightly yellow microcrystalline solid (4.60 g, 94% yield). mp 49°C. ^{1}H NMR (400 MHz, C6D6): δ 3.26 [sept, 2H, C*H*Me2], 3.06 [s, 12H, GaN(C*H*$_3$)$_2$], 2.28 [s, 6H, CN(C*H*$_3$)$_2$], 1.03 [d, 12H, CH(C*H*$_3$)$_2$]. ^{13}C NMR (C_6D_6): δ 167.8 [*C*N$_3$], 45.3 [*C*HMe$_2$], 42.6 [GaN(*C*H$_3$)$_2$], 38.9 [(*C*H$_3$)$_2$N], 24.5 [CH(*C*H$_3$)$_2$]. Mass spectra *m/e* (relative abundance): 328 (0.1) M+. Anal. Calcd for $C_{13}H_{32}GaN_5$: C, 47.58; H, 9.83; N, 21.34. Found: C, 47.96; H, 10.13; N, 21.05.

2.1.5 Gallium bisguanidinate monoamide

$[Me_2NC(N^iPr)_2]_2GaNMe_2$ (5). In a 50 mL flask, $Ga_2(NMe_2)_6$ (2.00 g, 4.95 mmol) was dissolved in 20 mL of hexane. The dropwise addition of diisopropylcarbodiimide (2.50 g, 19.81 mmol) to this solution resulted in a clear, slightly yellow solution, which was stirred overnight. The volatiles were removed in vacuo leaving a thick liquid with a slightly yellow colour. Cooling the solution to -30°C overnight resulted in the formation of a slightly yellow solid mass (4.425 g, 98% crude yield based on **5**). Further purification was required because ^{1}H NMR indicated the presence of a small amount of compound **6** as an impurity. The solid was dissolved in toluene and left to crystallize by slow evaporation of the solvent at -30°C Compound **5** was collected as clear, colourless crystals (1.858 g, 89% yield). mp 45°C ^{1}H NMR (400 MHz, C_6D_6): δ 3.56 [sept, 4H, C*H*Me$_2$], 2.93 [s, 6H, GaN(C*H*$_3$)$_2$], 2.52 [s, 12H, CN(C*H*$_3$)$_2$], 1.34 [d, 24H, CH(C*H*$_3$)$_2$]. ^{13}C NMR (400 MHz, C_6D_6): δ 167.70 [N*C*NMe$_2$], 46.68 [N*C*HMe$_2$], 41.95 [GaN(*C*H$_3$)$_2$], 40.01 [CN(*C*H$_3$)$_2$], 24.92 [CH(*C*H$_3$)$_2$]. Anal. Calcd for $C_{20}H_{46}GaN_7$: C, 52.87; H, 10.20; N, 21.58. Found: C, 53.10; H, 10.18; N, 21.88.

2.1.6 Gallium trisguanidinate

$[Me_2NC(N^iPr)_2]_3Ga$ (6). In a 50 mL flask, $Ga_2(NMe_2)_6$ (2.02 g, 5.00 mmol) was dissolved in about 10 mL of hexane. Diisopropylcarbodiimide (4.05 g, 32.09 mmol, slight excess) was added dropwise to the solution, resulting in a translucent, slightly yellow liquid. A clear, white microcrystalline solid formed overnight and was collected by filtration. The mother liquor was left to recrystallized by slow evaporation of the solvent at room temperature for 2 days. Additional crystals of **6** were collected by filtration (combined yield: 4.49 g, 77% yield). mp 137°C. ^{1}H NMR (200 MHz, C6D6): δ

3.74 [sept, 6H, C*H*Me$_2$], 2.65 [s, 18H, CN(C*H*$_3$)$_2$], 1.46 [br, 16H, CH(C*H*$_3$)$_2$], 1.39 [br, 16H, CH(C*H*$_3$)$_2$]. ^{13}C NMR (400 MHz, C_6D_6): δ 166.51 [N*C*NMe$_2$], 46.69 [N*C*HMe$_2$], 40.08 [CN(*C*H$_3$)$_2$], 26.20 [CH(*C*H$_3$)$_2$], 24.66 [CH(*C*H$_3$)$_2$]. Anal. Calcd for $C_{27}H_{60}GaN_9$: C, 55.86; H, 10.42; N, 21.71. Found: C, 55.81; H, 10.22; N, 21.84.

2.1.7 Aluminum bisguanidinate monochloride

[Me$_2$NC(N^{i}Pr)$_2$]$_2$AlCl (7). In a 50 mL flask, [Me$_2$NC(N^{i}Pr)$_2$]$_3$Al (**6**; 4.00 g, 7.44 mmol) was dissolved in 15 mL of hexane. In a separate 50 mL flask, $AlCl_3$ (0.496 g, 3.72 mmol) was suspended in 5 mL of hexane and then dissolved by adding ether dropwise (approximately 10 mL). The $AlCl_3$ solution was added to the solution of **6**, and the reaction mixture was stirred overnight. The solvent was partially removed in vacuo and cooled to -30°C. Compound **7** was collected as clear colourless crystals (2.19 g, 49% yield). ^{1}H NMR (400 MHz, C_6D_6): δ 3.50 [sept, 4H, C*H*Me$_2$], 2.39 [s, 12H, CN(C*H*$_3$)$_2$], 1.40 [d, 24H, CH(C*H*$_3$)$_2$]. ^{13}C NMR (400 MHz, C_6D_6): δ 170.29 [N*C*NMe$_2$], 45.44 [N*C*HMe$_2$], 38.90 [CN- (*C*H$_3$)$_2$], 24.09 [CH(*C*H$_3$)$_2$]. Mass spectra *m/e* (relative abundance): 402 (1.8) M+. Anal. Calcd for $C_{18}H_{40}AlClN_6$: C, 53.65; H, 10.00; N, 20.85. Found: C, 53.71; H, 10.36; N, 21.06.

2.1.8 Aluminum monoguanidinate dichloride

[Me$_2$NC(N^{i}Pr)$_2$]AlCl$_2$ (8). In a 50 mL flask, [Me$_2$NC(N^{i}Pr)$_2$]$_2$AlCl (**7**; 2.16 g, 5.36 mmol) was dissolved in about 20 mL of hexane. In a separate 50 mL flask, $AlCl_3$ (0.848 g, 7.44 mmol) was suspended in about 5 mL of hexane and then dissolved by adding ether dropwise (about 10 mL). The $AlCl_3$ solution was added to the solution of **7** and

stirred overnight. After purification, compound **8** was collected as clear colourless crystals (2.18 g, 76% yield). ^{1}H NMR (400 MHz, C_6D_6): δ 3.06 [sept, 2H, C*H*Me$_2$], 1.99 [s, 6H, CN(C*H*$_3$)$_2$], 1.04 [d, 12H, CH(C*H*$_3$)$_2$]. Mass spectra *m/e* (relative abundance): 267 (4.3) M+.

Structural Determinations for Compounds 1-7. Single crystals were mounted on thin glass fibers using viscous oil and then cooled to the data collection temperature. Crystal data and details of the measurements are included in the Supporting Information. Data were collected on a Bruker AXS SMART 1k CCD diffractometer using 0.3° ω scans at 0, 90, and 180° in ϕ. Unit-cell parameters were determined from 60 data frames collected at different sections of the Ewald sphere. Semiempirical absorption corrections based on equivalent reflections were applied. The structures were solved by direct methods, completed with difference Fourier syntheses, and refined with full-matrix least-squares procedures based on F^2. All non-hydrogen atoms were refined with anisotropic displacement parameters. All hydrogen atoms were treated as idealized contributions. All scattering factors and anomalous dispersion factors are contained in the SHELXTL 5.1 program library.

2.2 Results

The homoleptic amido dimers $M_2(NMe_2)_6$ (M = Al, Ga) react readily with two, four, and six equivalents of diisopropylcarbodiimide to yield six new guanidinato complexes of these group 13 metals (Figure 20). Compounds **1-6** have been isolated in good to excellent yields as clear and colourless crystalline materials with relatively low melting points for the mono and bis(guanidinato) species (45-70°C) and somewhat higher values (137 and 193°C) for the tris(guanidinato) compounds. Each of these compounds exhibited distinctive ^1H and ^{13}C NMR signatures that are consistent with the suggested formulations. In addition, the similarities between these spectra indicate that the related Al and Ga compounds have analogous solution structures.

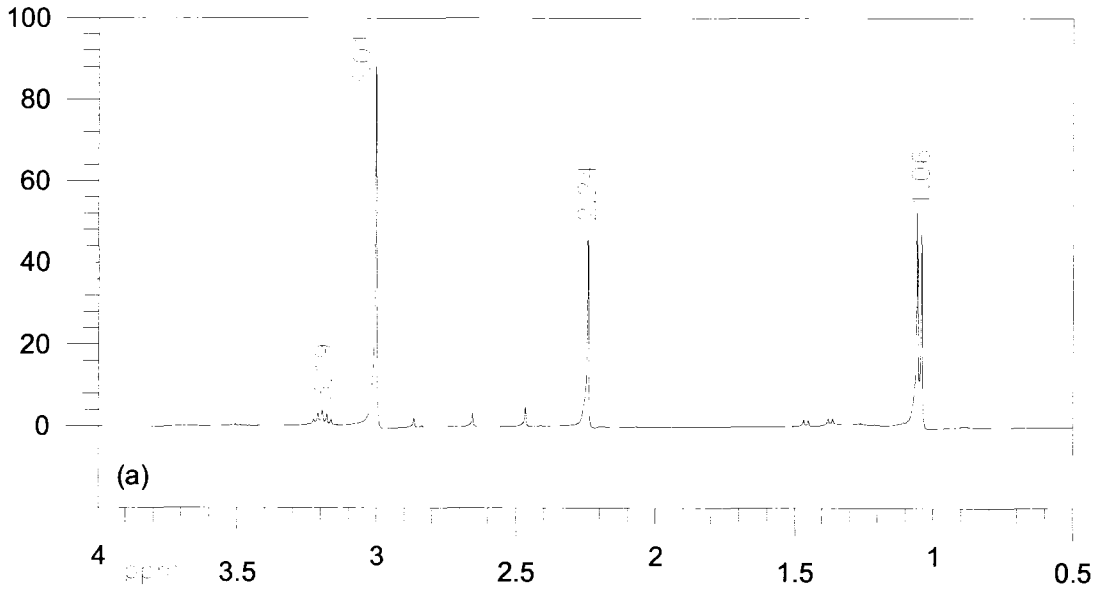

Figure 14: *^1H-NMR Spectra for* Compound **1**. *(For peak assignments, refer to Experimental)*

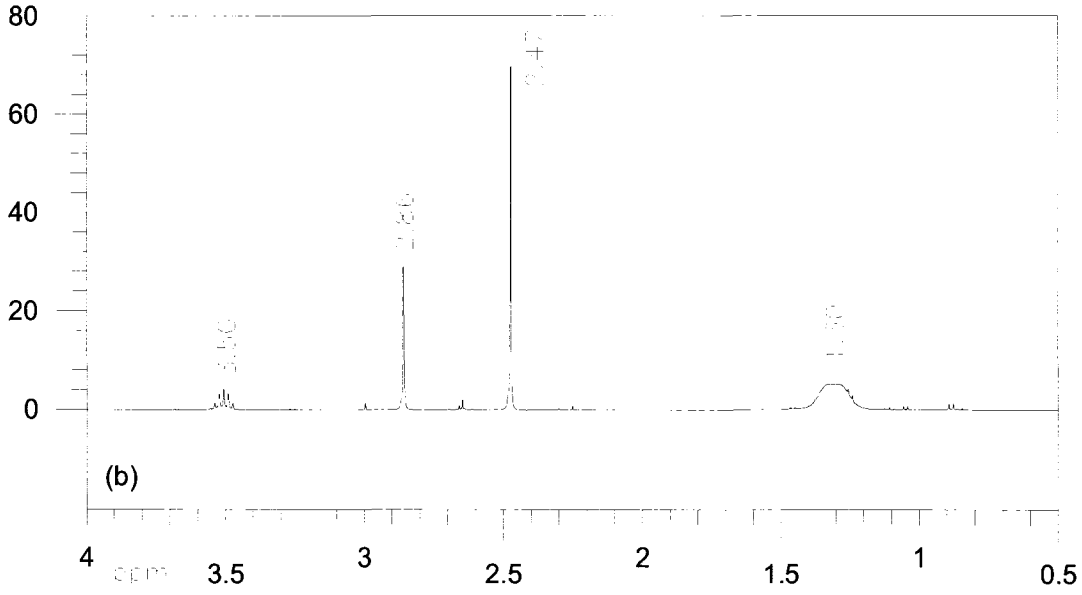

Figure 15: *^{1}H-NMR Spectra for* Compound **2**. *(For peak assignments, refer to Experimental)*

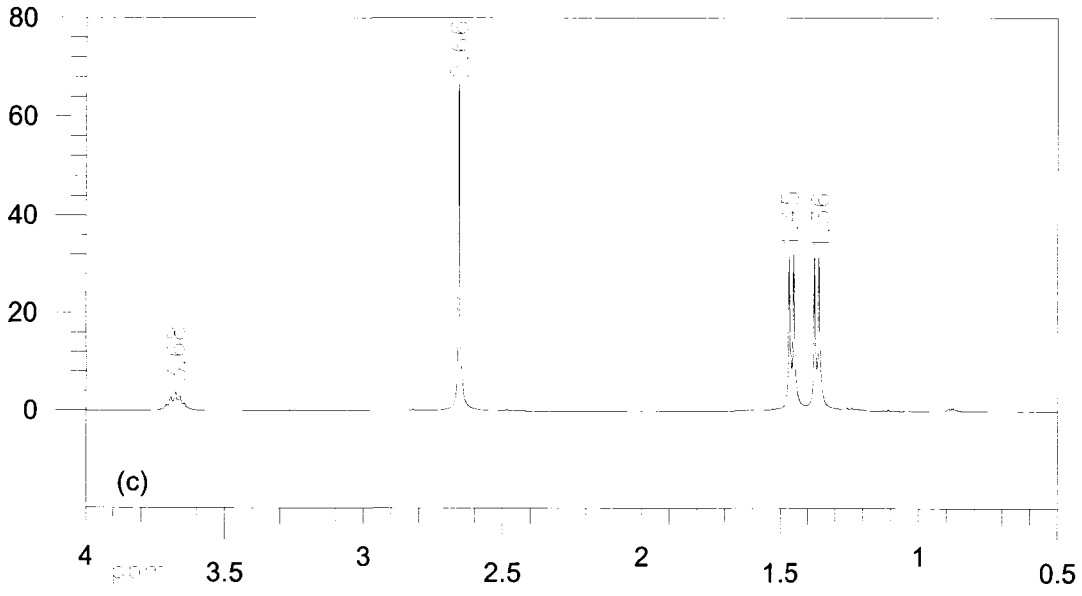

Figure 16: *^{1}H-NMR Spectra for* Compound **3**. *(For peak assignments, refer to Experimental)*

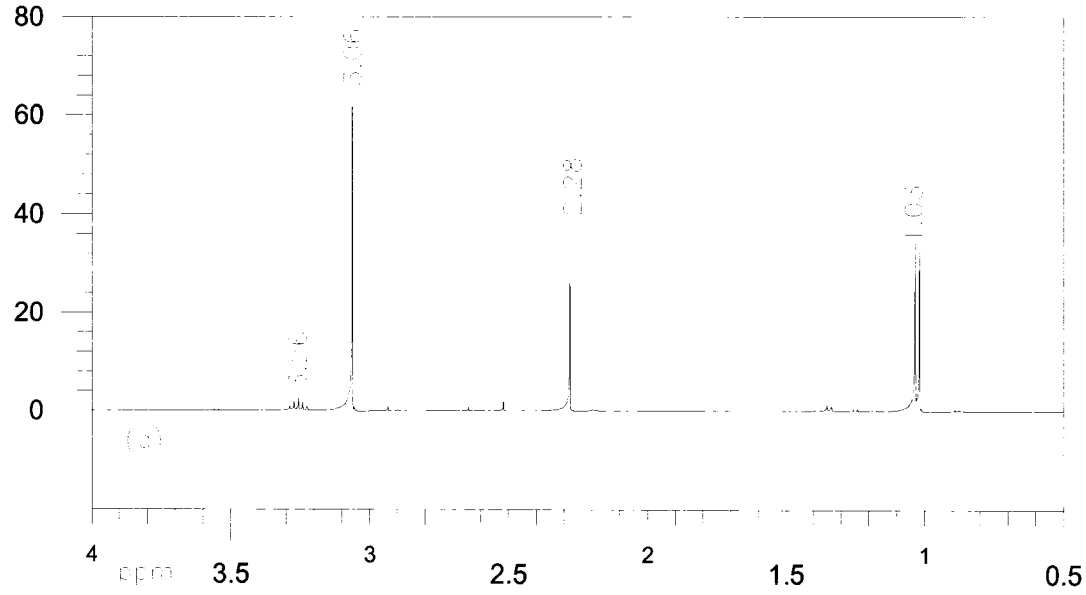

Figure 17: *^{1}H-NMR Spectra for* Compound **4**. *(For peak assignments, refer to Experimental)*

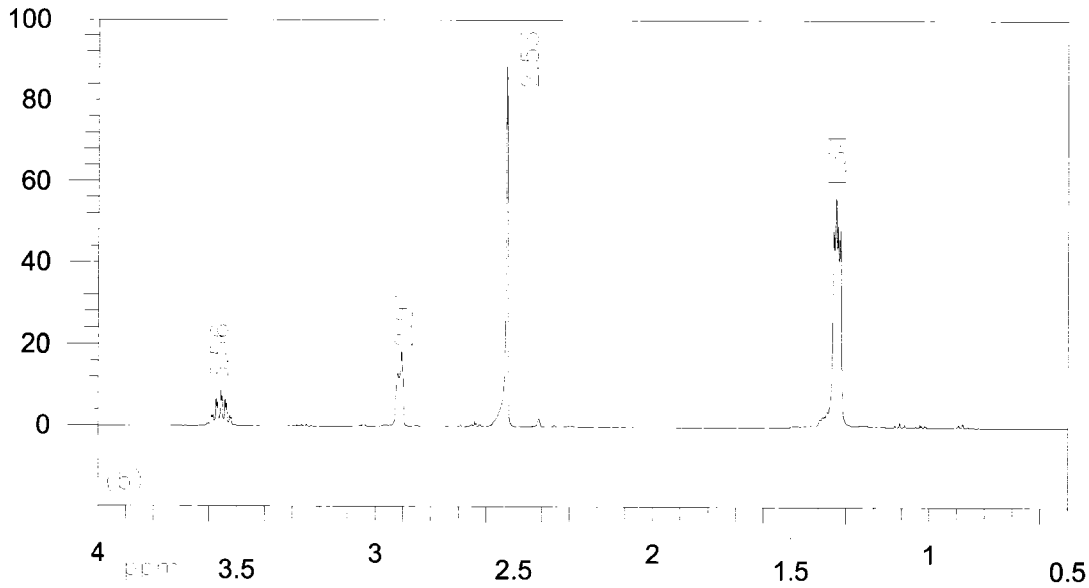

Figure 18: *^{1}H-NMR Spectra for* Compound **5**. *(For peak assignments, refer to Experimental)*

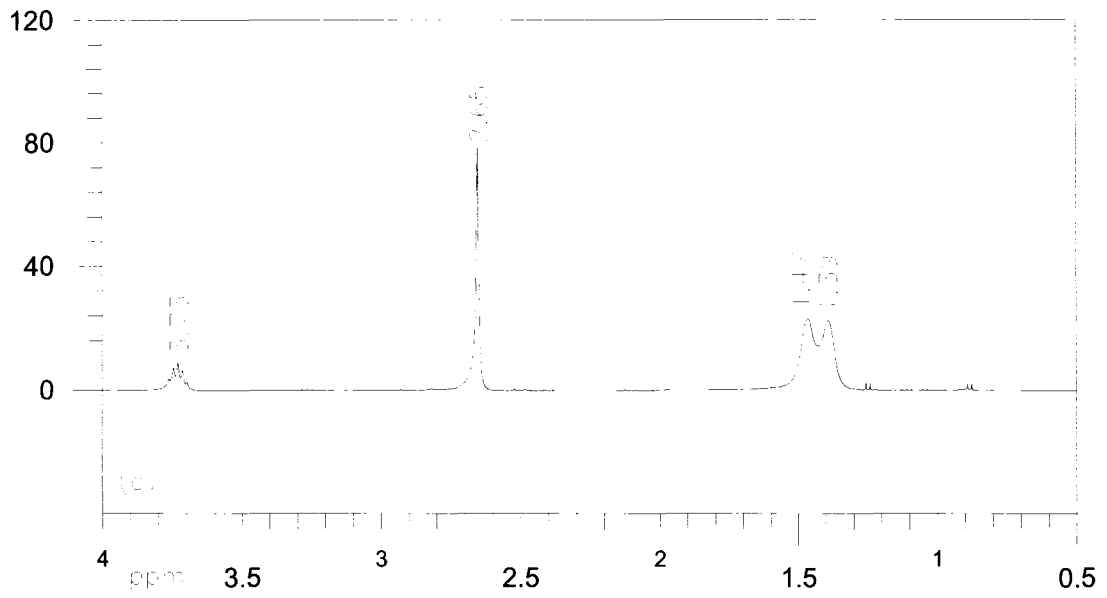

Figure 19: *^{1}H-NMR Spectra for* Compound **6**. *(For peak assignments, refer to Experimental)*

Compounds **1 - 6** have been characterized by single-crystal X-ray diffraction analysis, and these results are presented below. As anticipated for a monomeric, distorted tetrahedral metal environment of C_{2V} symmetry, the NMR spectra of compounds **1** and **4** (Figure 14 and Figure 17) indicate a single environment for the ^{i}Pr substituents of the guanidinato ligand. The guanidinate ligand is "fluxional", in that it is able to equilibrate their diastereotopic methyl groups through a dechelation/rechelation of the ligand (*a* and *a'* in Figure 20). This implies that there is only one environment, and as will be shown, there is little steric congestion around the metal centre.

As more guanidinate ligands are added around the metal centre, it would be expected that more steric hindrance is present due to the bulk of the ligand. This can be seen ^{1}H-NMR spectras of **2** and **5** (Figure 15 and Figure 18), where fluxional the solution structures become evident by the broadening of the peaks for the ^{i}Pr substituent in the NMR. These peaks are broad because there is more than one environment for the

isopropyl groups, but that they are fluctuating at a rate that is approaching the timeframe of the NMR. The static distorted trigonal bipyramidal structures of these two compounds should yield two spectroscopically distinguished ^{i}Pr substituents with four diastereotopic Me groups corresponding to *a, a', e,* and *e'*, as indicated in Figure 20. The experimental observation of a single set of isopropyl resonances including only one doublet for the methyl groups in **1** and **4** indicates a fluxional process that equilibrates axial/equatorial sites as well as the two faces of the guanidinato ligand.[28]

This effect can be further explored by examination of the ^{1}H-NMRs of compounds **3** and **6** (Figure 16 and Figure 19). There are now two signals for the methyls in the isopropyl groups for compound **3**, and two broad peaks for compound **6**. This implies that there are two separate environments for compound **3**, and a fluxional environment for compound **6.**

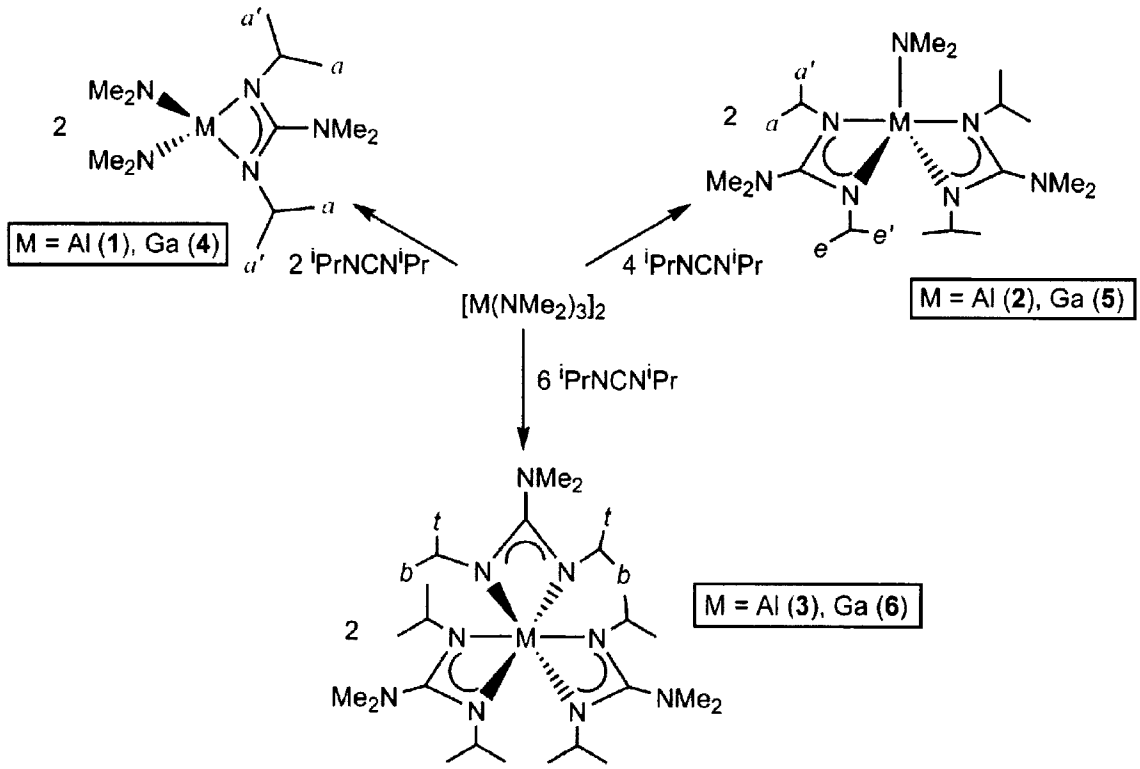

Figure 20: *Stoichiometric Control of Carbodiimide Insertion into Metal-Amide Bonds.*

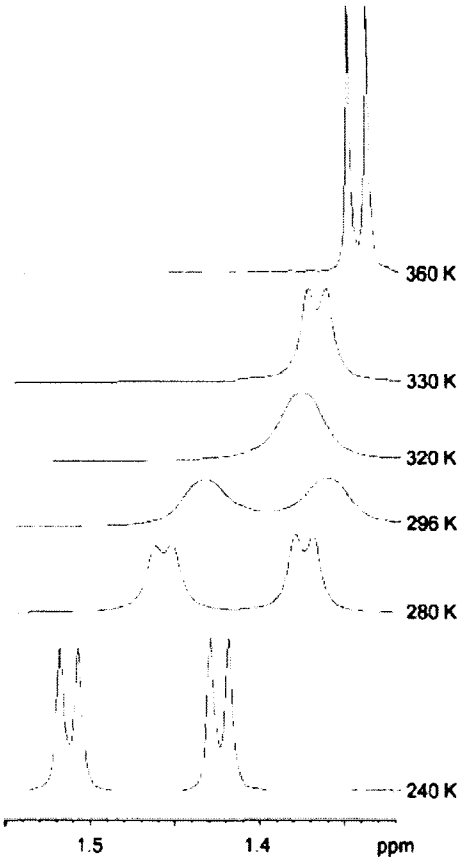

Figure 21: *Variable temperature ^{1}H NMR study of compound **6**, focusing on the spectral region for the methyl signals for the isopropyl groups of the guanidinato ligands.*

The ^{1}H NMR spectra of the six coordinate, tris(chelate) complexes **3** and **6** support the structure shown in Figure 20 and, in the case of compound **6**, display features consistent with a dynamic solution structure. The spectra for this species display one equivalent environment for the three guanidinato ligands, and the appearance of one singlet for the dimethylamido group is consistent with the free rotation of the C-NMe_2 bond at room temperature. Furthermore, the ^{i}Pr groups of **3** display a single septet for the CH moiety with two well-resolved doublets at 1.46 and 1.37 ppm having equal intensity for the methyl groups. This is entirely consistent with the limiting structure illustrated in Figure 20 in which the two inequivalent Me groups are indicated as *t* and *b*. A dynamic

process that exchanges these diastereotopic methyl groups is evident in the spectra of **6** in which two broad resonances appear at 1.36 and 1.44 ppm in the room temperature ^{1}H NMR spectrum. Variable-temperature ^{1}H NMR spectra further support the fluxional behavior by demonstrating the limiting structures. As seen in Figure 21, when a sample of **6** is cooled below 280 K, the static limit is reached and the isopropyl moieties now appear as two doublets for two inequivalent Me groups. Above 320 K, an exchange process that equilibrates the two ligand faces becomes dominant and renders the Me groups equivalent. These observations are reversible. This is attributed to the lower barrier to rotation that is seen for **6** compared to **3**. This larger barrier is a result of the larger metal centre and longer M-N bonds, which decrease the steric interaction with the isopropyl group.

A closer examination of the reactions illustrated in Figure 20 revealed an unexpected pathway that relates the mono-, bis-, and tris(guanidinato) species. During the preparations of these species, it was noted that the reaction of the starting amido compounds with six equivalents of diisopropylcarbodiimide to form the tris(guanidinato) complexes occurred very rapidly, in a matter of minutes. In contrast, reactions between the aluminum amido dimers and two equivalents of carbodiimide required much longer reaction times in order to isolate high yields of compound **1**. The gallium compounds show the same reactivity.

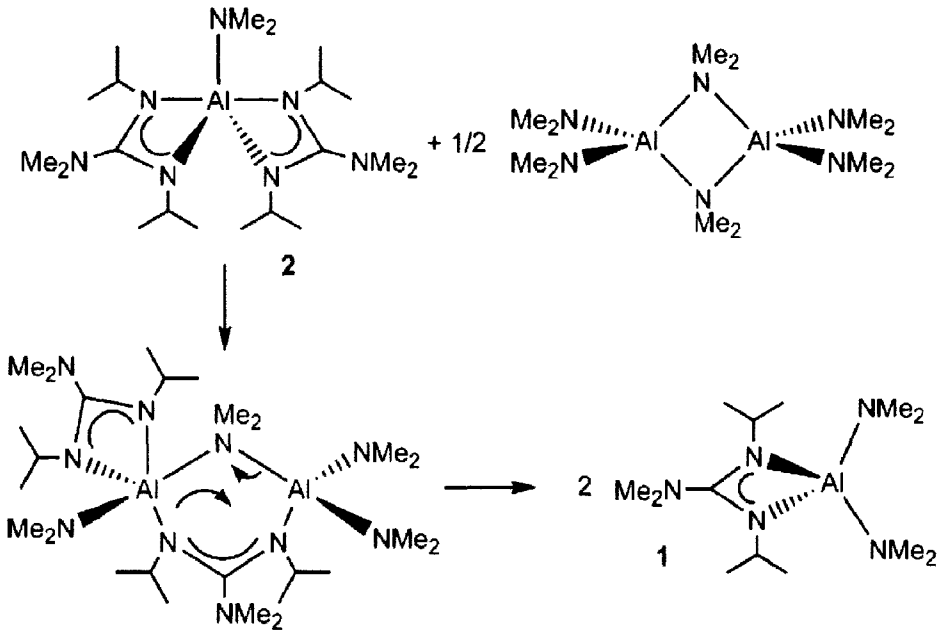

Figure 22: *Proposed Ligand Exchange Mechanism as the Slow Step in Amido Guanidinate Formation.*[16]

An examination of the ^{1}H NMR spectra of the 1:2 reaction mixtures at early reaction times indicated a complex reaction mixture that contained small amounts of the target compound ([(^{i}PrN)$_2$CNMe$_2$]Al(NMe$_2$)$_2$) (Compounds **1-3**) as well as significant amounts of the bis- and tris(guanidinato) compound [(^{i}PrN)$_2$CNMe$_2$]$_2$AlNMe$_2$ and [(^{i}PrN)$_2$CNMe$_2$]$_3$Al, respectively (Compounds **1-3**). These mixtures also contained an appropriate amount of unreacted homoleptic amido compound. Furthermore, the reaction with six equivalents of carbodiimide and the amido starting material gave (in minutes) the octahedral tris(guanidinato) species **3**, and ^{1}H NMR spectra that were taken at early stages of the reaction showed only the presence of **3** as well as the starting amido complex. In addition, monitoring the reaction of amido starting material with four equivalents of carbodiimide by ^{1}H NMR indicated the presence of the tris(guanidinato) complex **3** along with unreacted homoleptic amido species. Compound **1** was not

observed in these reaction mixtures. Allowing these reactions to proceed overnight led, ultimately, to the formation of the expected bis(guanidinato) compound **2**. This set of observations suggests that the insertion of diisopropylcarbodiimide with $M_2(NMe_2)_6$ proceeds rapidly to produce the triply inserted octahedral products and unreacted starting materials. These products then undergo a ligand exchange reaction on a much slower time scale (over several hours) to ultimately lead to stoichiometrically controlled products. In all cases, the syntheses of **1** and **4** can be carried out in high yield, provided that sufficient time is allowed for the ligand redistribution and incorporation of starting amido complexes. These observations can be attributed to a slow reaction of the dinuclear homoleptic amido species with carbodiimide. Once this dimer is cleaved and has undergone an insertion of carbodiimide, subsequent insertions are very rapid and proceed to generate the tris(guanidinato) species. Then a slower guanidinate exchange with amide occurs that leads to the desired product. In an effort to shed some light on the process of ligand exchange, the reaction between the tris(guanidinato) complexes and the amido species were carried out using **3** with $AlCl_3$ in stoichiometric ratios of 2:1 and 1:2. The sole isolated products in these two reactions were $[(^iPrN)_2CNMe_2]_2AlCl$ (**7**) and $[(^iPrN)_2CNMe_2]AlCl_2$ (**8**), respectively. Compound **8** was previously synthesized $[(^iPrN)_2CNMe_2]AlCl_2$ using salt metathesis between the lithium guanidinate and aluminum chloride,[24] while complex **7** is a new species that was isolated in excellent yield and which we have fully characterized spectroscopically and through single-crystal X-ray diffraction. There was no evidence for the formation of free carbodiimide in either of these reactions, nor were there any products that possessed chloroamidinate ligands, $(^iPrN)_2CCl^-$, which would have indicated carbodiimide insertion into the Al-Cl bond.[11]

2.3 Crystal Structure

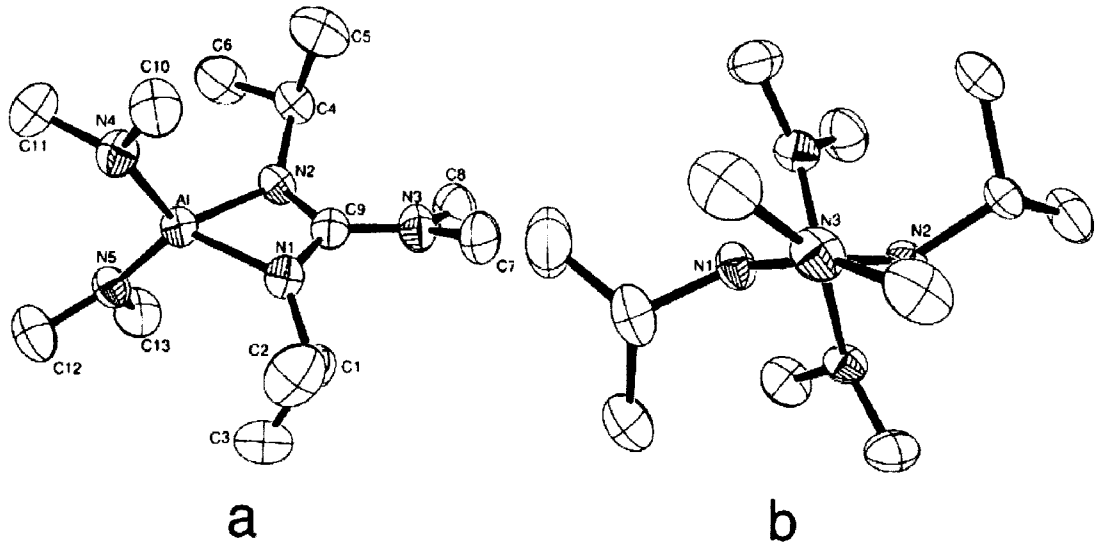

Figure 23: *(a) Molecular structure and atom numbering scheme for compound 1. (b) A view of the structure of 1 in the guanidinate plane along the Al-C9-N3 axis is provided in order to show the distortion of N1 and N2 from planarity and the angle between the NMe_2 plane and the N1-C9-N2 plane. Hydrogen atoms have been omitted in every case for clarity, and thermal ellipsoids are shown at 50% probability.*

The single-crystal X-ray diffraction results for compounds **1** and **4** are summarized in Figure 23 and Table 1 and 2. The structure of **4** is excluded from Figure 23 because it is isostructural with **1**.

Table 1: *Crystallographic data for compounds 1 – 7.*

compound	**1**	**2**	**3**	**4**
empirical formula	$C_{13}H_{32}AlN_5$	$C_{20}H_{46}AlN_7$	$C_{27}H_{60}AlN_9$	$C_{13}H_{32}GaN_5$
formula weight	285.42	205.81	537.82	328.16
T (K)	203(2)	206(2)	203(2)	203(2)
λ (Å)	0.71073	0.71073	0.71073	0.71073
crystal system	monoclinic	monoclinic	cubic	monoclinic
space group	$P2_1/n$	$C2/c$	$I\bar{4}3d$	$P2_1/n$
unit cell dimensions (Å, deg)	a = 8.729(5)	a = 16.510(4)	a = 23.5593(1)	a = 8.754(2)
	b = 15.213(7)	b = 8.754(2)	b =23.5593(1)	b =14.065(3)
	c = 13.902(4)	c = 18.025(4)	c =23.5593(1)	c =15.400(4)
	β = 97.25(4)°	β = 93.185(4)°	β = 101.801(4)°	
V (Å^3)	1831.4(2)	2601.2(1)	13076(1)	1856.1(8)

compound	**5**	**6**	**7**
empirical formula	$C_{20}H_{46}GaN_7$	$C_{27}H_{60}GaN_9$	$C_{18}H_{40}AlClN_6$
formula weight	454.36	580.56	402.99
T (K)	205(2)	203(2)	207(2)
λ (Å)	0.71073	0.71073	0.71073
crystal system	monoclinic	cubic	monoclinic
space group	$P2_1/n$	$I\bar{4}3d$	$P2_1/c$
unit cell dimensions (Å, deg)	a = 9.345(3)	a = 23.7146(1)	a = 13.796(4)
	b = 16.241(4)	b = 23.7146(1)	b = 9.531(3)
	c = 17.524(5)	c = 23.7146(1)	c = 18.470(5)
	β = 5.327(6)°	β = 98.809(4)°	
V (Å^3)	2648.1(1)	13337(2)	2400.0(1)
Z	4	16	4
F (calculated; g/cm^3)	1.14	1.157	1.115
R1, wR2[a]	0.0568, 0.1059	0.0294, 0.0711	0.0460, 0.1068

[a] $[I > 2\sigma(I)]$. $R1 = \Sigma||F^o| - |F_c||/\Sigma|F^o|$. $wR2 = (\Sigma\omega(|F^o| - |F_c|)^2/\Sigma\omega|F^o|^2)^{1/2}$

These results confirmed the monomeric nature of these compounds and demonstrated that the Al and Ga species have very similar structures, as was suggested by the NMR data. For example, both complexes have the metal centre in a distorted tetrahedral environment provided by two amido ligands and a bidentate guanidinate ligand, with the restricted bite angle of the guanidinate ligand as the origin of the major deviations from ideality. In **1**, the amido nitrogen centers N4 and N5 are planar, as indicated by the sum of the angles around these atoms of 358.5° and 358.1°, respectively.

The analogous amido centers in the Ga species (**2**) are less planar (Σ angles: N4 = 356.0°; N5 = 352.9°), which is a common contrasting feature of the amido compounds of these two elements.[29] The most remarkable feature of the structures of **1** and **4** is the deviation from planarity for the guanidinate N1 and N2 centers. Specifically, for compound **1**, the sum of angles around N1 and N2 is 351° and 346°, respectively, and the corresponding values in **4** were found to be 353° and 344°. The effect is obvious when the structure is viewed in the plane of the guanidinate ligand, and this view for complex **1** is shown in Figure 14b. It is also noteworthy that all three C-N bonds in the guanidinate ligands of **1** and **4** are equivalent with average values of 1.348(4) Å for **1** and 1.357(6) Å for **4**. The remaining bonding parameters within the guanidinate ligands in **1** and **4** are in accord with previously reported structures of guanidinate complexes.[24,25]

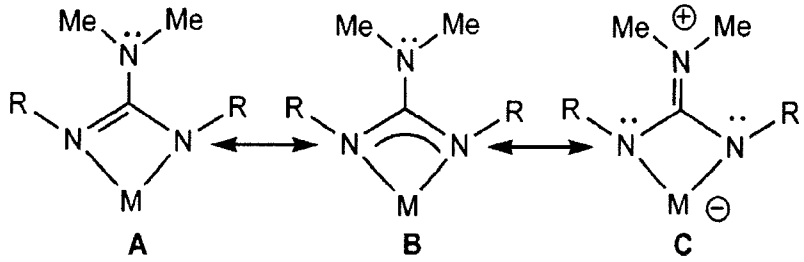

Figure 24: *Possible Resonance Structures Showing the Planarity of the Exocyclic Nitrogen in the Guanidinate.*

An understanding of the bonding parameters within the guanidinate ligands may be provided by a consideration of the potential resonance structures A-C (Figure 24). A characteristic feature of guanidinate ligands is the presence of the exocyclic amido moiety that is capable of donating lone pair electron density to the central carbon of the chelate ring, thus, stabilizing a zwitterionic resonance structure. This resonance structure leads to increased electron donation to the metal and leaves lone pair electron density on the two metal-bound N centers (C). If this contribution is significant, two structural

features should be observed. The exocyclic amide's nitrogen centre should be planar and sp^2 hybridized, allowing the p-orbital-localized lone pair to overlap with the NCN moiety. In addition, there should be a small torsion angle between the plane NR'_2 group and that defined by the NCN chelate for maximum π bonding. The structural features observed in **1** and **4** support a significant contribution from structure C. As well as a planar N(3) centre, the torsion angles defined by M-N1-C9-N2 are 2.6° for both **1** and **4**, showing that the ring nitrogens are both non-planar. The non-planar N(1) and N(2) centers are also consistent with structure C and a significant lone pair electron density on these centers leading to the observed pyramidalization. Finally, the torsion angle of N1-C9-N3- C7 is 23.5° in **1** and 36.1° in **4**, along with the N3-C9 bond length, suggests that the exocyclic nitrogen is experiencing some degree of π bonding with the chelate ring in both structures. The single-crystal X-ray diffraction results for compounds **2**, **5**, and **7** are summarized in Figure 3 and Tables 1 and 2. The structure of **5** is excluded from Figure 3 because it is isostructural with **2**. As it is, compounds **2**, **5**, and **7** share several structural similarities. Only **2** possesses a strict C_2 axis of symmetry, but the slight deviations of **3** and **7** suggest that all three complexes can be treated as having metal centers in pseudotrigonal bipyramidal coordination geometries of approximately C_2 symmetry.

For trigonal bipyramidal structures (tbp), a factor τ,[30] can be used to determine the degree that the structure is close to the ideal structure. This can also be considered the percentage of tbp versus the percentage of square pyramidal. The value of τ is determined by two angles, α and β where α is the angle between two bonds in the equatorial plane and β is the angle between the two axial bonds. Ideally in a tbp

structure, α should be 120° and β should be 180°. The formula for calculating tau is τ = (β – α)/60° where τ must be between 0 and 1 since 1 represents the ideal tbp case and 0 represents the 'ideal' square pyramidal. For compound **3**, τ = 0.61, and for compound **5**, τ = 0.59. The major geometrical cause of the deviation from a trigonal bipyramidal structure in both cases was the bending of the axial angle (157.3° in **3** and 157.2 in **5**) due to the low bite angles of the chelate ligands (67.2 in **3** and 65.0° in **5**) compared to the ideal 90° found in an undistorted trigonal bipyramidal geometry.

All three compounds possess three equatorial groups (e.g., N2, N9, and N9b for **2**; N3, N10, and N17 for **5**; and Cl, N4, and N15 for **7**) that are coplanar with the sum of the angles between these groups equal to 360°. The angle between the pseudoaxial positions shows a similar distortion for the three complexes, which we attribute to the limited bite angle of the guanidinato ligand. In compounds **2** and **5**, this angle is observed to be 157°, with a slightly larger value of 166° for **7**. As expected, the equatorial M-N bonds in **2**, **5**, and **7** were shorter than the axial distances. These differences are larger for **2** (δ= 0.19 Å) and **5** (δ= 0.17 Å) than for **7** (δ= 0.06 Å). The guanidinate ligands in these compounds exhibit similar bonding parameters as those seen in complexes **1** and **3**, which again suggests a significant contribution of resonance structure C (Figure 15) to the bonding in these bis- (guanidinato) compounds. Specifically, the guanidinate exocyclic N centers are planar and the dihedral angles between these groups and the chelate NCN planes fall in the range of 28.1-46.4°. These two features are consistent with the partial π conjugation of these groups. In addition, the nitrogen centers in the guanidinato chelate ring show similar deviations from planarity. For example, in **2**, the sum of angles around N4 and N9

are 355° and 352°, respectively. The analogous angles in **5** have an average value of 352°, and those in **7** have an average value of 351°. There appears to be some correlation of this distortion with steric congestion at the metal centre, with the larger deformations observed for **2** and the smallest for **5**. Single-crystal X-ray diffraction analyses have also been carried out on the hexacoordinate species **3** and **6**. The results of these studies are illustrated in Figure 4 and summarized in Tables 1 and 2. Both structures are symmetrical pseudooctahedral species possessing only one unique guanidinate ligand, as indicated by the NMR data. The limitations imposed by the bite angle of the guanidinate ligand (65.72° in **3** and 63.86° in **6**) lead to distortions of these structures from ideal octahedral geometries. Thus, the ideal 180° axes are reduced to 157.4° and 154.7° in **3** and **6**, respectively. The M-N bonds are only slightly longer than those observed for **1-4**, with values of 2.024 Å in **3** and 2.086 Å and 2.095 Å in **6**. In contrast to the mono- and bis(guanidinato) species, the chelate rings in these complexes are planar, as indicated by the near-zero values of the M-N1-C9-N2 angles (Table 2). The C-NMe_2 groups are planar (Σ angles = 357.7°) in both species. The relatively large angles between the exocyclic nitrogen planes and the NCN planes for these compounds, with values of 40.3° for **3** and 41.0° for **6**, and the longer C9-N3 bond lengths indicate less π overlap between these moieties. These features indicate that B, rather than C (Scheme 3), is the dominant ligand resonance structure for these two species. Given the potential of species **1-6** in vapour-phase thin film syntheses (chemical vapour deposition or atomic layer deposition), it is pertinent to note that the mass spectrometry data for **1**, **2**, and **4** indicate the presence of a parent ion peak for the mononuclear species and no evidence of dimerization or oligomerization. The highest mass peak observed for compound **3** had an *m/e* value of

283, which is consistent with the fragment $[Me_2NC(N^iPr)_2]Ga(NMe_2)^+$ derived by the loss of one dimethylamido group from a monomeric species. All six of these compounds exhibited clean melting points and may offer the potential to be used as liquid precursors.

2.4 Thermolysis

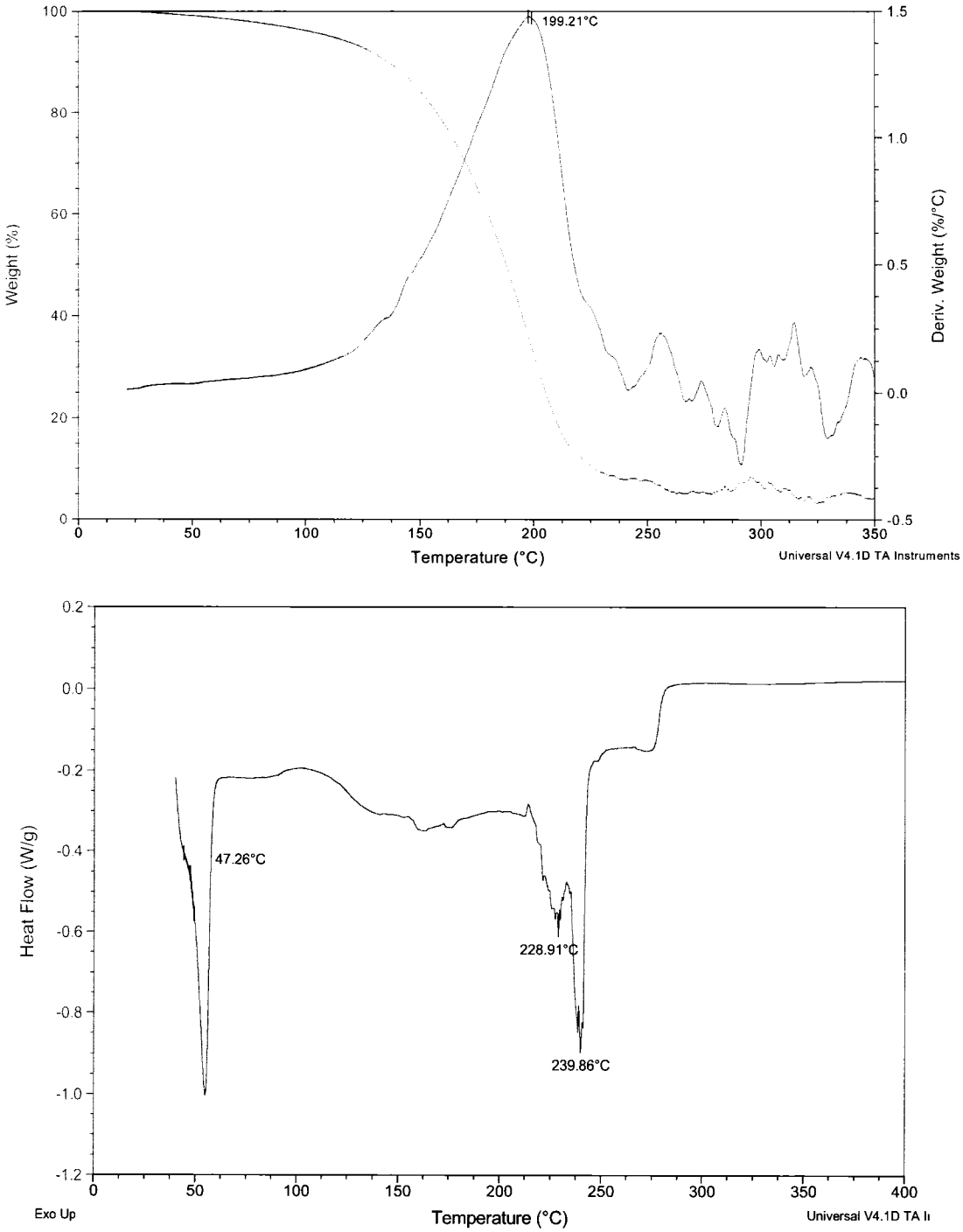

Figure 25: *TGA and DSC of Compound 1.*

The TGA for compound **1** shows a slow onset of volatilization and a relatively steep decline until the depletion of the sample occurs and the weight-loss ceases. This is

what a TGA typically looks like for compounds that do not undergo any thermal decomposition. The curve which is not the percent weight loss in the TGA of Figure 25 is the negative of the derivative of the % weight loss. This can show more clearly how many volatilization events are occurring. Ideally, the derivative of the weight loss is should have only one peak, implying only one thermal event, i.e. vaporization. The DSC shows four major endothermic events, the first is due to the melting point at 47°C which was confirmed by bench-top methods. The second broad peak is likely due to volatilization since volatilization occurs over a range of temperatures, and so the endotherm associated with this process likewise extended over a temperature range. As well, the volatilization endotherm appears to correspond with the onset of volatilization. The third and fourth peaks are likely due to a decomposition. This might account for the unsettled baseline following the volatilization event in the TG curve.

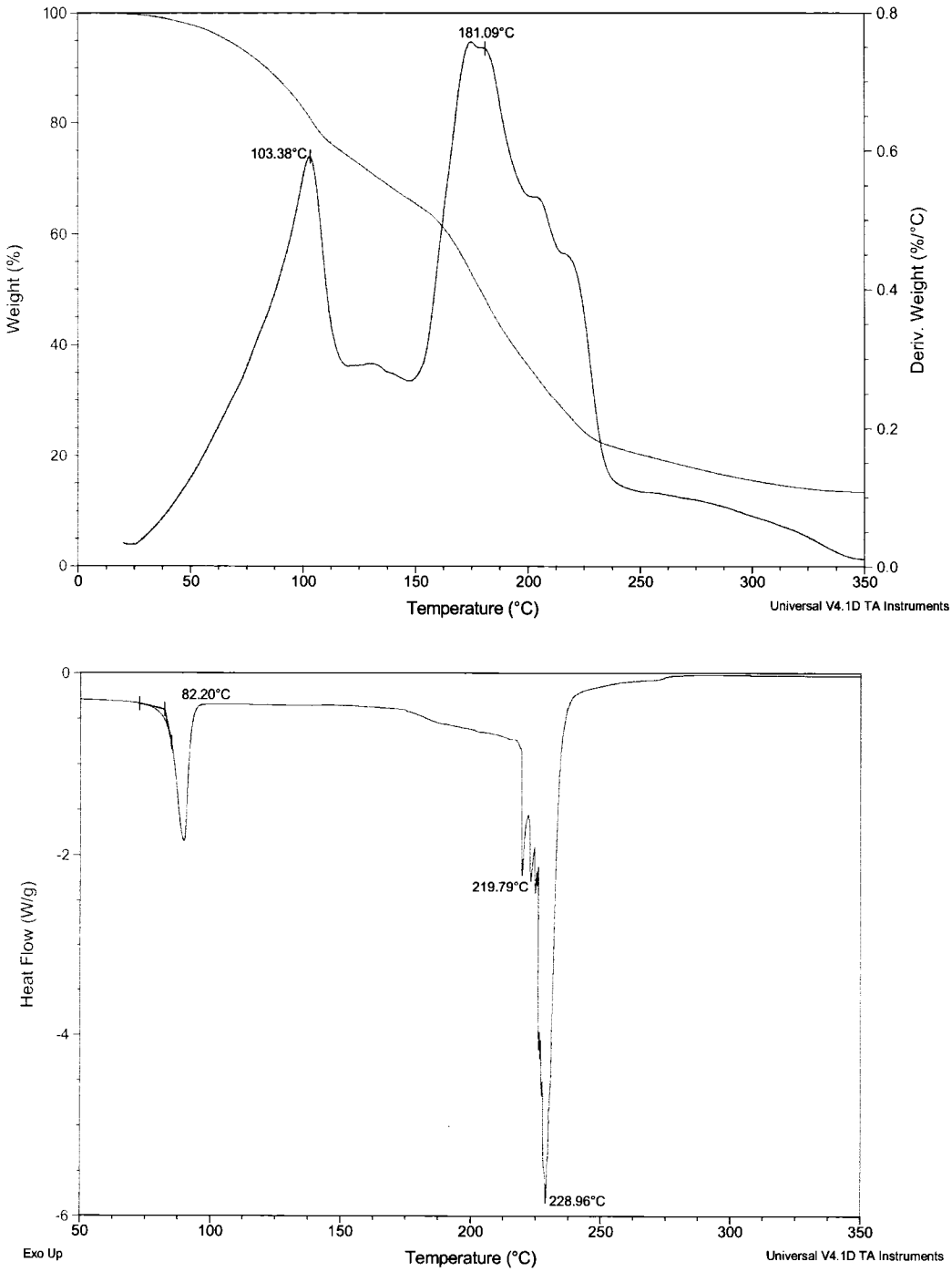

Figure 26: *TGA and DSC of Compound 2.*

The TGA for compound **2** is not nearly as simple as it is for compound **1**. It is clear that there are at least two major processes happening where one is volatilization and the other is decomposition. These features overlapped in the TG, and thus the

decomposition, which may have produced a volatile species as well, complicated the simple thermolysis expected for this compound. The VT-NMR shown earlier (Figure 21) showed the first clues as to what the thermal decomposition route would be for the mono- and bis-substituted guanidinates. Not shown in the earlier discussion (due to simplicity), the NMR peaks for diisopropyl carbodiimide, were present at high temperatures. This result implied that the reverse of the synthetic route of carbodiimide insertion was occurring. This "carbodiimide deinsertion" would only occur in bis and tris substituted compounds, so this may be one of the decomposition routes evident in the thermolysis data.

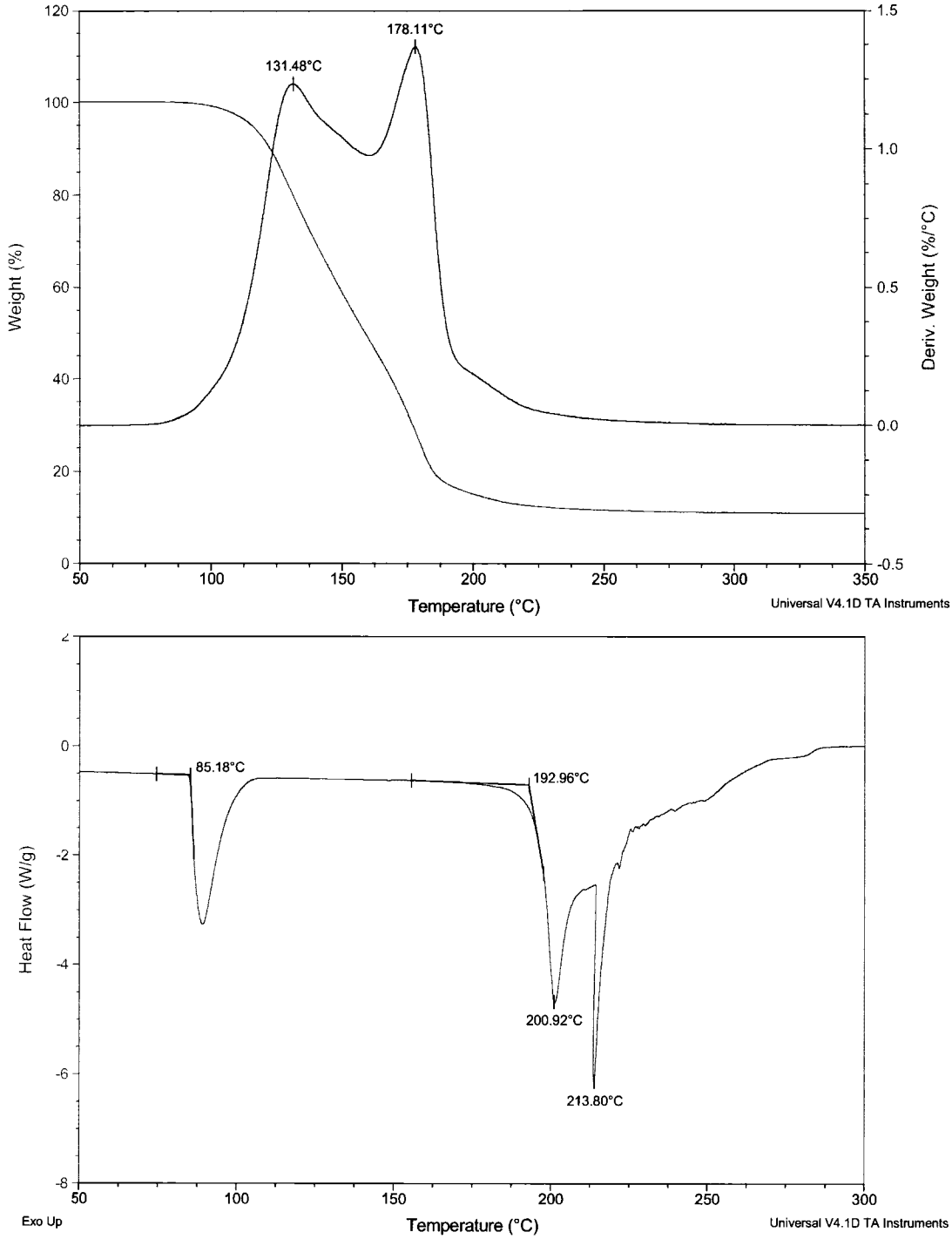

Figure 27: *TGA and DSC of Compound 3.*

More evidence for the carbodiimide deinsertion decomposition route is the mass spec of the bis and tris substituted compounds. The peaks for carbodiimide are clearly shown in

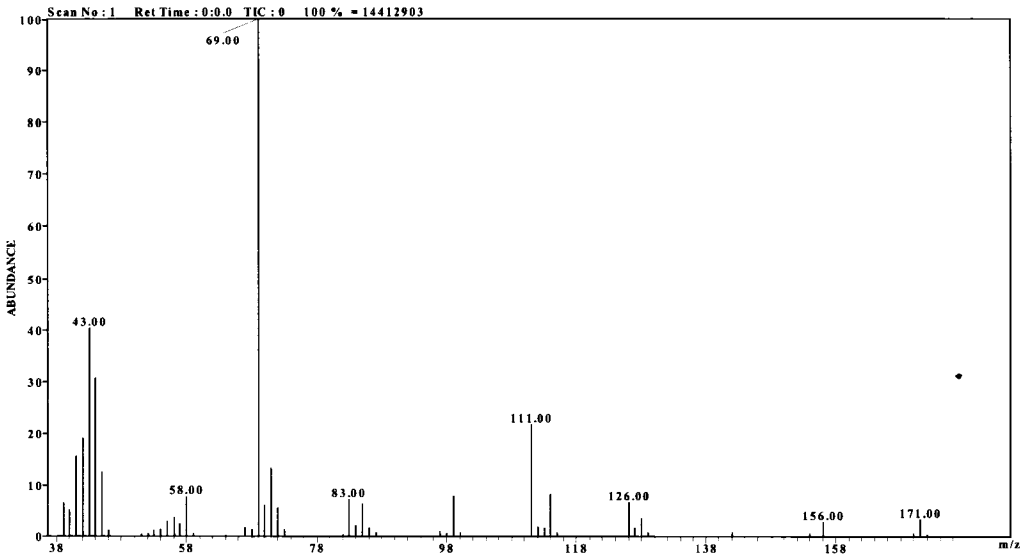

.

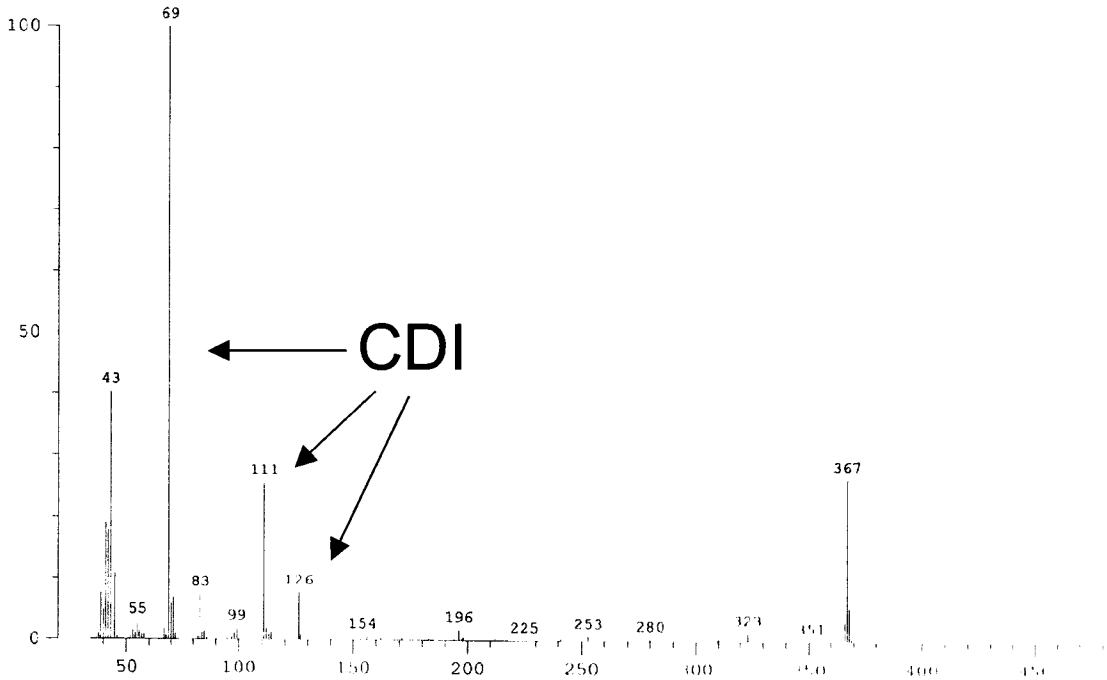

Figure 28: *Mass Spectrum of compound 3 showing CDI deinsertion*

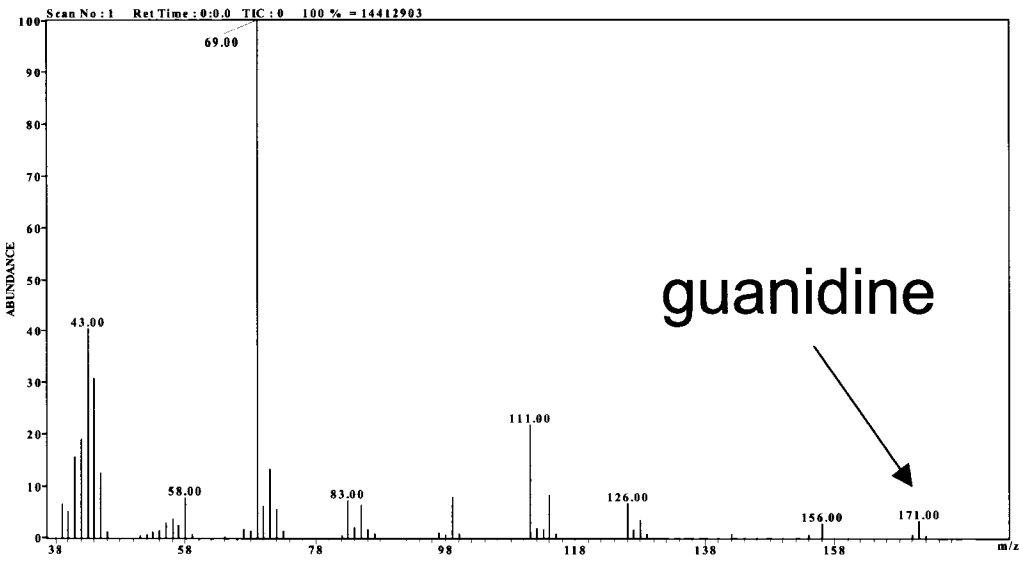

Figure 29: *Mass Spectrum of compound 1 showing no CDI deinsertion.*

In contrast, the mass spec of compound **1** (Figure 29) has a peak for guanidine. This shows that the CDI peaks in the mass spec are due to CDI deinsertion, since there are no parent guanidine peaks in the mass spec for compound **3**.

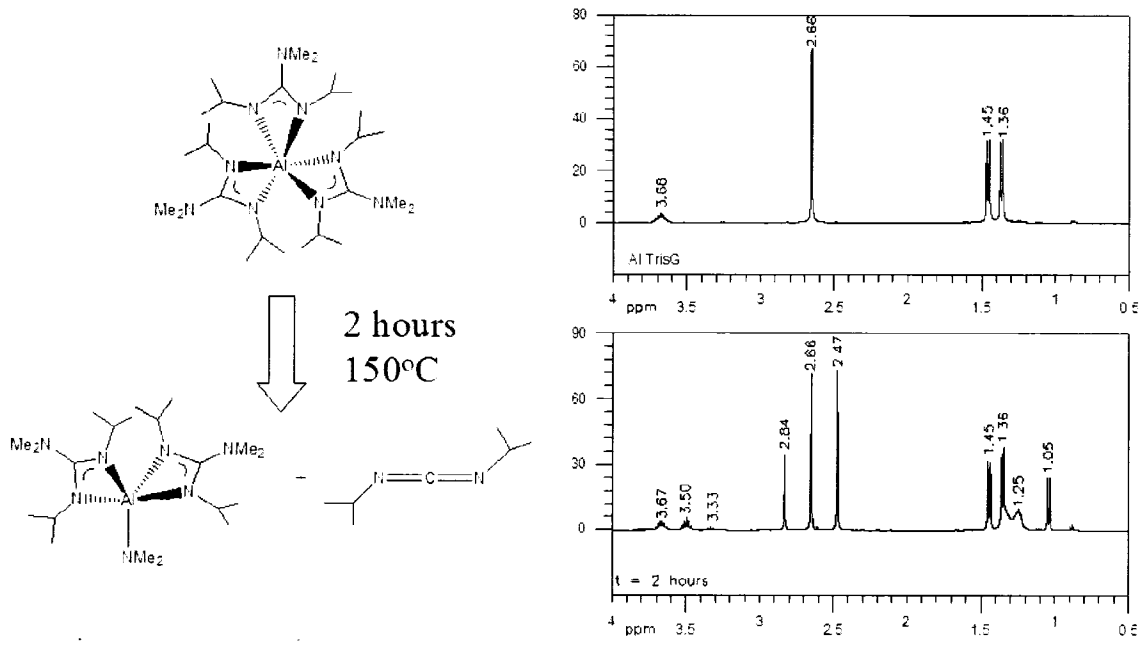

Figure 30: *Decomposition of compound 3 in a sealed NMR tube.*

Further evidence for CDI deinsertion is the NMR spectra of compound **3** in a sealed NMR tube. The NMR tube containing compound **3** and the solvent (C_6D_6) was frozen in liquid nitrogen and sealed. After it thawed, an ^{1}H-NMR was taken at room temperature, then again after being heated for 2 hours at 150°C. The result shows additional presence of compound **2** and CDI.

2.5 Reactivity at a Surface

Exposure experiments were performed with compound **1** and **3** to see if they would react with silica. The experimental set-up involved the silica powder being placed in a porous boat inside a hot-walled chamber. The precursor was volatilized in a heated chamber, and the silica was exposed to the volatilized precursor under low pressure. High surface area silica is used so that the reaction may be easily characterized using FT-IR or MAS-NMR. The silica was held at 180°C for both compounds **1** and **3**. Pure silica powder is very white, so one of the first observations that implied reaction may have occurred was the darkening of the powder to a light yellow colour. This only occurred with compound **1**, which suggested that compound **1** may have reacted and compound **3** may not have reacted. The reaction of either compound **1** or **3** with the silica should show C-H stretching modes in an IR spectra of the substrate, compared to that of pure silica (which has no C-H bonds). These stretching modes were only found to be present in the reaction with compound **1** (Figure 31), further suggesting that compound **3** did not react to form a chemisorbed surface species.

Compound **1** differs from compound **3** in that there are two possible reactive 'anchoring' ligands (the amido ligands) available to react with surface sites on the silica. Compound **3** must react through the guanidinato ligand, which is less reactive due to

chelation with the metal centre. This can account for the different reactivities between compound **1** and **2**.

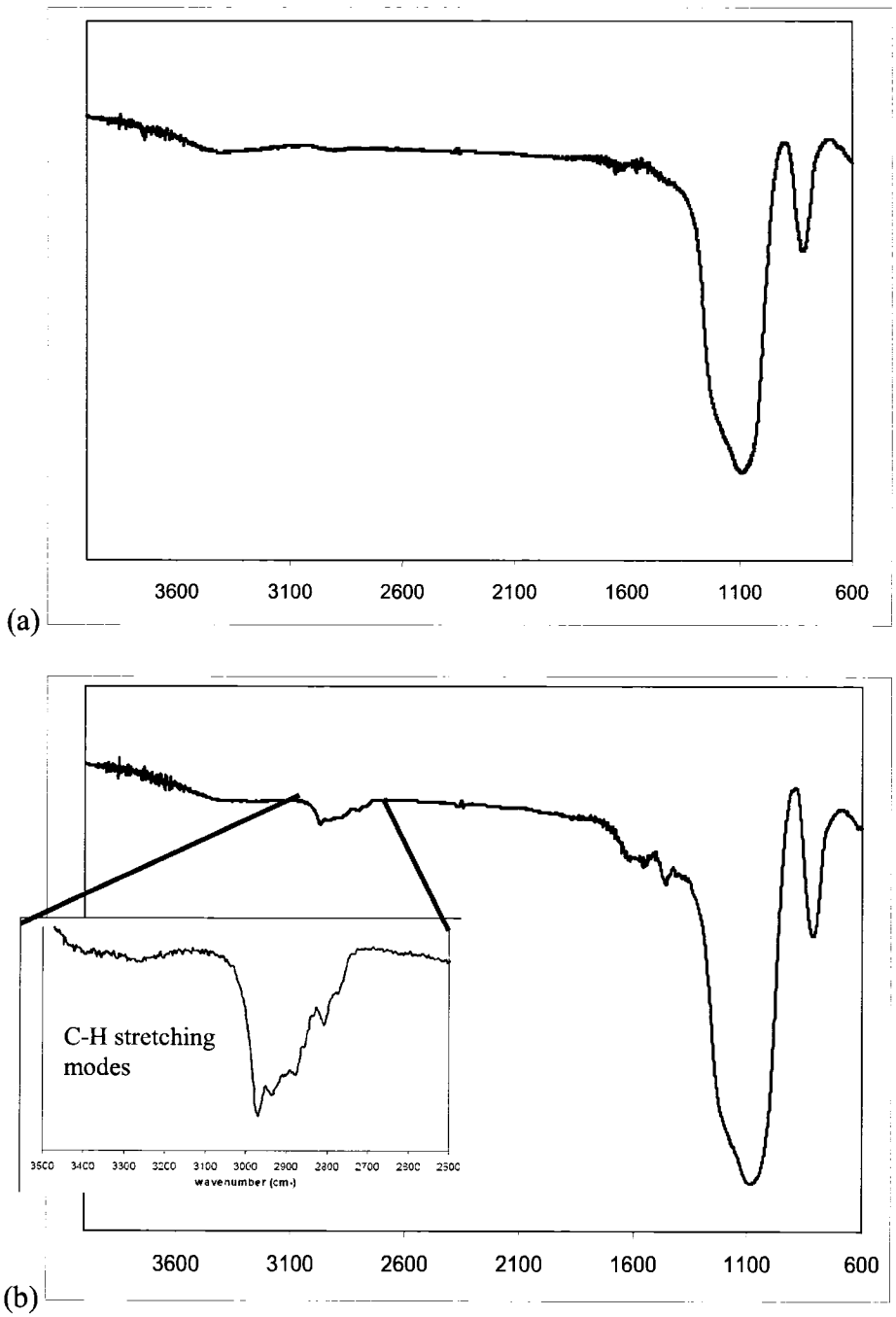

Figure 31: *(a) Unreacted Silica Powder, (b) Silica Reacted with Compound **1**.*

3 Ipip compounds

3.1 Introduction

One problem with amidinato type ligands is that carbodiimide deinsertion may occur under high temperatures. This can lead to unpredictable reactions occurring in the vapour phase, resulting in an unknown vapour concentration and uncontrolled vapour composition. It is best to use a ligand that is thermally stable with respect to deinsertion to allow for predictable reactions within the hot-walled furnace.

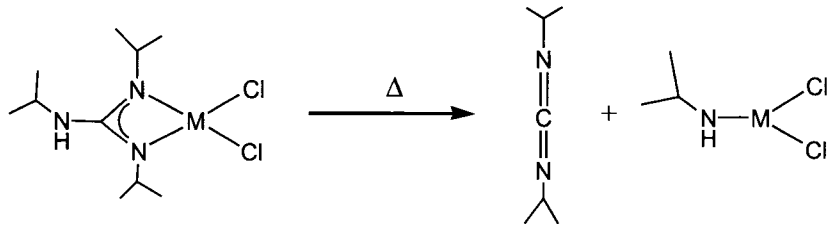

Figure 32: *Carbodiimide deinsertion reaction.*

One such ligand that might inhibit this thermal decomposition could have a chemical linkage between the exocyclic position to the chelating amine. This would make the deinsertion reaction difficult due to sterics and geometrical constraint. However, if deinsertion were to occur, the two would still be linked, which not affect the reaction as much as if the two were to separate completely. An example of this type of ligand is N-isopropyl iminopyrrolidine (ipip) (Figure 33).

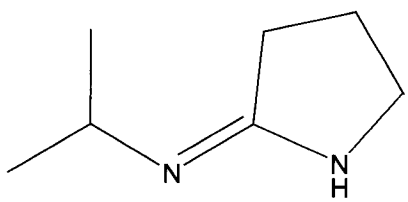

Figure 33: *N-isopropyl iminopyrrolidine (ipip) ligand.*

This ligand has the same chelate possibility to a metal centre as an amidinate, however with the carbon chains linked, it should eliminate the possibility of deinsertion.

3.2 Synthesis

3.2.1 N-isopropyl iminopyrrolidine (ipip)

[^{i}PrNC$_4$H$_6$NH] (9) The synthesis of the ipip ligand was a modified synthesis of a similar compound from Pederson, 1980.[31] 9.71 g (68.4 mmol) P_2O_5 was added to 17.46 g (205.2 mmol) pyrrolidone over a 15-minute period while stirring vigorously to create a homogenous suspension. This was stirred for 1 hour to allow the solution to cool. 24.61 g (416.3 mmol) isopropyl amine was added to the mixture and refluxed overnight at 230°C while stirring vigorously. After cooling, 100 mL of ice was added to the reaction flask followed by 200 mL of 2 M NaOH. This was left to dissolve for 1 hour. The aqueous layer was extracted three times with 200 mL of ether. The ether solution was dried over $NaSO_4$. The ether was removed *in vacuo*. The solid was crystallized out of a small amount of hot hexane. Compound **9** was collected as clear, colourless crystals (7.04 g 27% yield). mp 93 °C. ^{1}H NMR (400 MHz, C_6D_6): δ 4.08 [sept, 1H, C*H*Me$_2$], 3.78 [trip, 2H, N(C*H*$_2$)(CH$_2$)], 1.89 [trip, 2H, C(C*H*$_2$)(CH$_2$)], 1.60 [quint, 2H, N(CH$_2$)(C*H*$_2$)], 1.02 [d, 6H, CH(C*H*$_3$)$_2$]. Mass spectra *m/e*: 126 (M^+).

Monoipip dimethyl Aluminum

[(CH$_2$)$_3$NCN^{i}Pr]$_2$Al$_2$ (10) 0.692 g (5.48 mmol) of N-isopropyl imino pyrrolidine was suspended in 20 mL of hexane was added dropwise to 2.74 mL (5.48 mmol) of $AlMe_3$ while being stirred. The solution effervesced and the remaining solid dissolved. This was stirred for thirty minutes and dried *in vacuo*. 0.73 g (73% crude yield) of slightly

yellow microcrystalline solid was collected. mp 82 °C. ^{1}H NMR (400 MHz, C_6D_6): δ 3.28 [sept, 2H, C*H*Me$_2$], 3.22 [trip, 4H, N(C*H*$_2$)(CH$_2$)], 1.93 [trip, 4H, C(C*H*$_2$)(CH$_2$)], 1.34 [quint, 4H, N(CH$_2$)(C*H*$_2$)], 1.16 [d, 12H, CH(C*H*$_3$)$_2$], -0.36 [s, 12H, Al(C*H*$_3$)$_2$].

3.2.2 Copper ipip

[(CH$_2$)$_3$NCN^{i}Pr]$_2$Cu$_2$ (11) 1.337 g (10.6 mmol) of isopropyl imino pyrrolidine was dissolved in 20 mL of ether. 1.06 mL (10.6 mmol) of BuLi was added dropwise to the solution and stirred for three hours. 1.049 g (10.6 mmol) of CuCl was slowly added to the solution and left to stir for four days. The solution was filtered and the solid was rinsed with 40 mL ether. 1.53g (76.5 % yield) ^{1}H NMR (400 MHz, C_6D_6): δ 3.34 [trip, 4H, N(C*H*$_2$)(CH$_2$)], 3.26 [trip, 4H, N(C*H*$_2$)(CH$_2$)], 2.03 [trip, 4H, C(C*H*$_2$)(CH$_2$)], 1.58 [broad, 4H, N(CH$_2$)(C*H*$_2$)], 1.20 [d, 12H, CH(C*H*$_3$)$_2$], 1.15 [d, 12H, CH(C*H*$_3$)$_2$].

Compound **9** was synthesized through a modified literature route (Figure 34).[31]

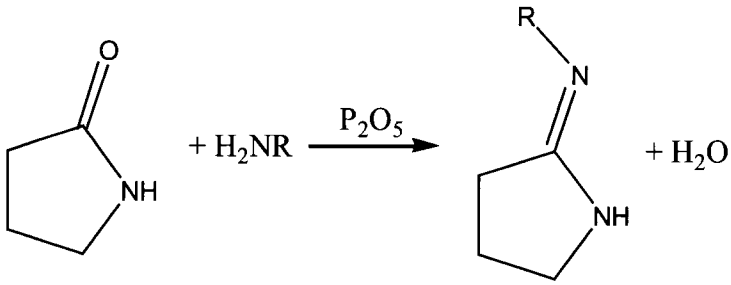

Figure 34: *Synthesis of the N-isopropyl iminopyrrolidine (ipip) ligand, where R =* ^{i}*Pr.*

This literature synthesis was for the aniline imine derivative of this compound. The synthesis with the isopropyl imine version proved to be a more difficult synthesis than the aniline version. The yield was typically around 10% however the highest was 27% as stated above. The reason for the low yield is unknown; attempted characterization of the residual material was unsuccessful. The amine used in the

synthesis ($^{i}PrNH_2$) is highly volatile, and the reaction was extremely exothermic. The low (and variable) yield could be due to the volatilization of this reactant. Any subsequent attempts to make this ligand should consider using the hydrochloride salt of the amine to restrict volatilization losses. However, since much of this reaction was performed outside of the drybox, it could be produced in large batches to yield a usable mass of ligand.

The aluminum tris ipip and copper ipip precursors (compounds **10** and **11**) were both synthesized via salt metathesis. The Hipip was reacted with BuLi *in situ* and subsequently reacted with $AlCl_3$ and CuCl respectively.

Compound **10** was synthesized very easily by the addition of the ipip ligand with TMA in a 1:1 ratio. The reactive methyls on the aluminum reacted with the fluxional hydrogen on the ipip releasing methane gas. The yield was fairly high at 73% and the melting point was low enough to be used as a liquid precursor in ALD.

3.3 Crystal Structure

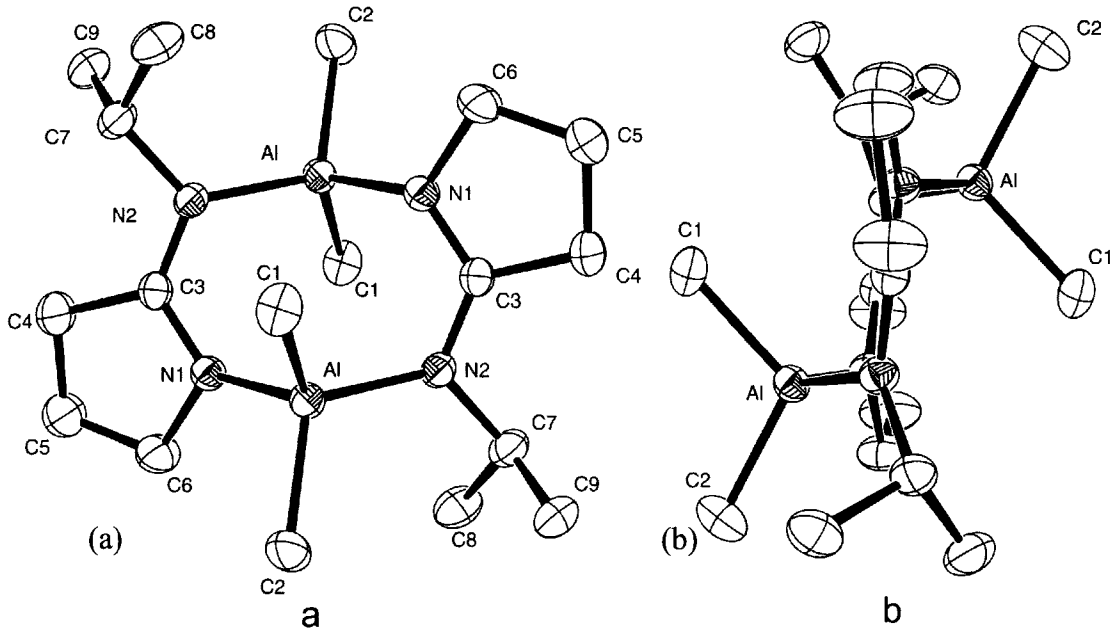

Figure 35: *(a) Molecular structure and atom numbering scheme for compound **10**. (b) A side view of the structure of Compound 10 along the amidinate-Al ring structure is provided in order to illustrate the chair conformation. Hydrogen atoms have been omitted in every case for clarity, and thermal ellipsoids are shown at 50% probability.*

Table 2 *Crystallographic data for compound **10**.*

Compound	**10**
empirical formula	$C_{18}H_{38}Al_2N_4$
formula weight	464.49
T (K)	205(2)
λ (Å)	0.71073
crystal system	monoclinic
space group	$P2_1/n$
unit cell dimensions (Å, deg)	a = 8.101(8)
	b = 8.521(9)
	c = 15.814(16)
	β = 93.618(15)°
V (Å^3)	1089.4(19)
Z	4
F (calculated; g/cm^3)	1.111
R1, wR2[a]	0.0543, 0.1853
[a] $[I > 2\sigma(I)]$. $R1 = \Sigma\|\|F°\| - \|F_c\|\|/\Sigma\|F°\|$. $wR2 = (\Sigma\omega(\|F°\| - \|F_c\|)^2/\Sigma\omega\|F°\|^2)^{1/2}$	

This data shows the unexpected result of a dimeric connectivity of the aluminum compound. The space group is $P2_1/n$, which means that is has a C_2 axis of symmetry. The NMR does not give any indication of the dimeric connectivity due to the symmetry of the compound. The Al centre had a distorted tetrahedral environment comprised of two methyl groups and the bonds to the nitrogens in the ipip ligand. The N1-Al-N2 bond angle was widened from ideal to 111.2°, however, the methyl groups were close to the ideal tetrahedral angle (C1-Al-C2 = 109.3°). The widening of the N1-Al-N2 angle was likely due to the flattening of the ring from the sp^2-hybridized nature of the carbon of the chelate ring. The chelating nitrogens and carbons are planar, as indicated by the sum of the angles around these atoms of (N1: 355.32°, N2: 357.5°, and C3: 359.97°). It is interesting to note that the dimer **10** was almost entirely planar except for the aluminum (along with it's methyl groups), which adopted positions above and below the plane of the ligand at an angle of 94.4° (i.e. the C3-N2-Al-N1 torsion angle = 94.4°). The chelate is very flat because of the participation of the central carbon (C3) in the π system within the ligand. However the nitrogens are slightly less than ideal to accommodate the geometry around the aluminum. There is a slight buckling of the sp^2-hybridized carbon (C5-C4-C3-N1 torsion angle = 12.1°) within the five-membered ring. This is most likely to allow for a slight twisting of the ring to accommodate the chelate to the aluminum. The aluminum may be participating in the π system of the ligand system by hyperconjugation with the chelating nitrogens.

Thermolysis

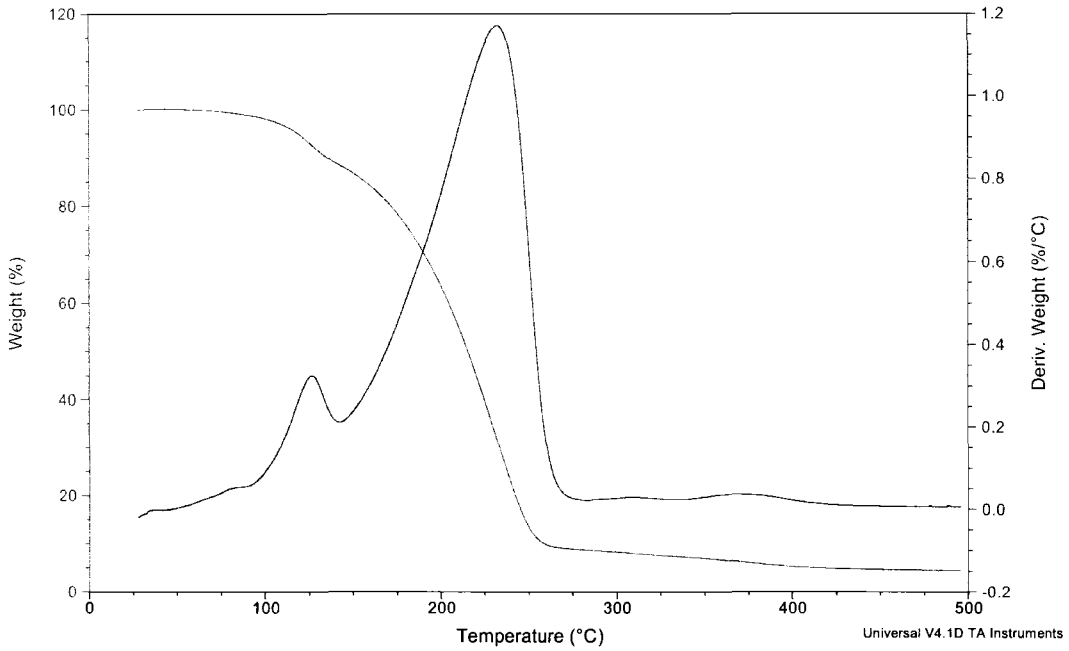

Figure 36: *Thermogravimetric Analysis of Compound **10**.*

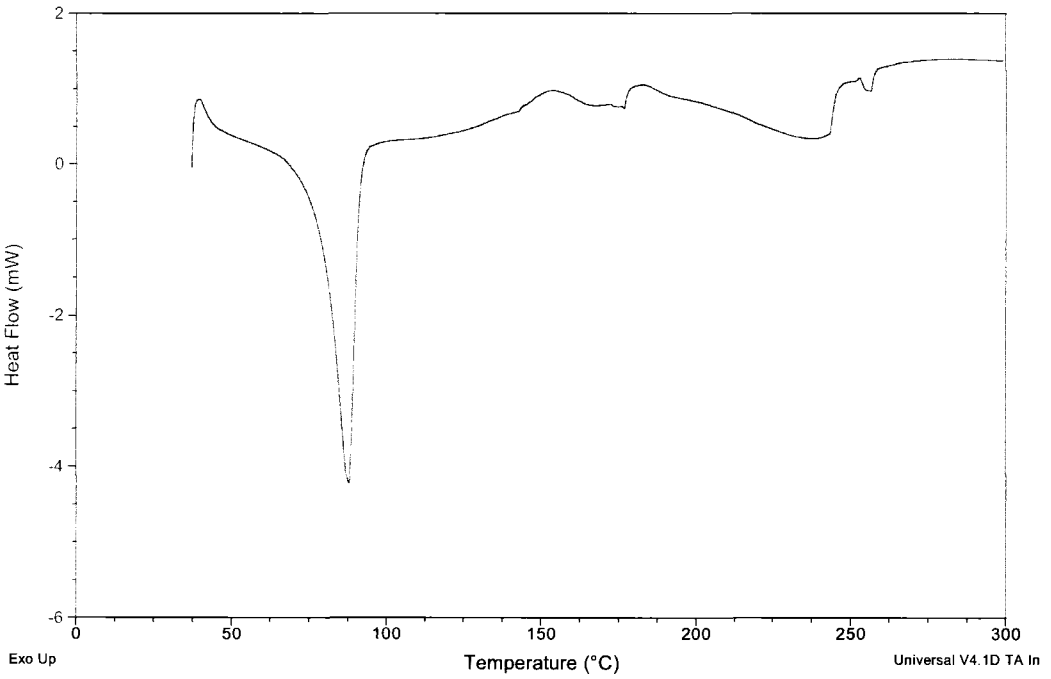

Figure 37: *Differential Scanning Calorimetry of Compound **10**.*

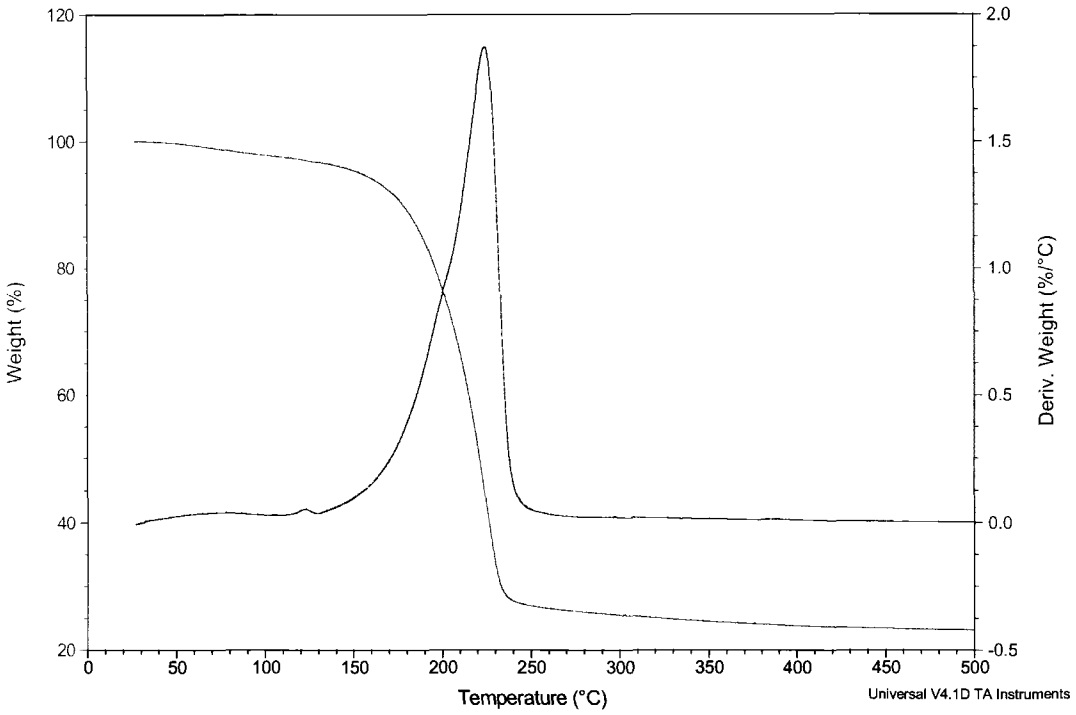

Figure 38: *Thermogravimetric Analysis of Compound 11.*

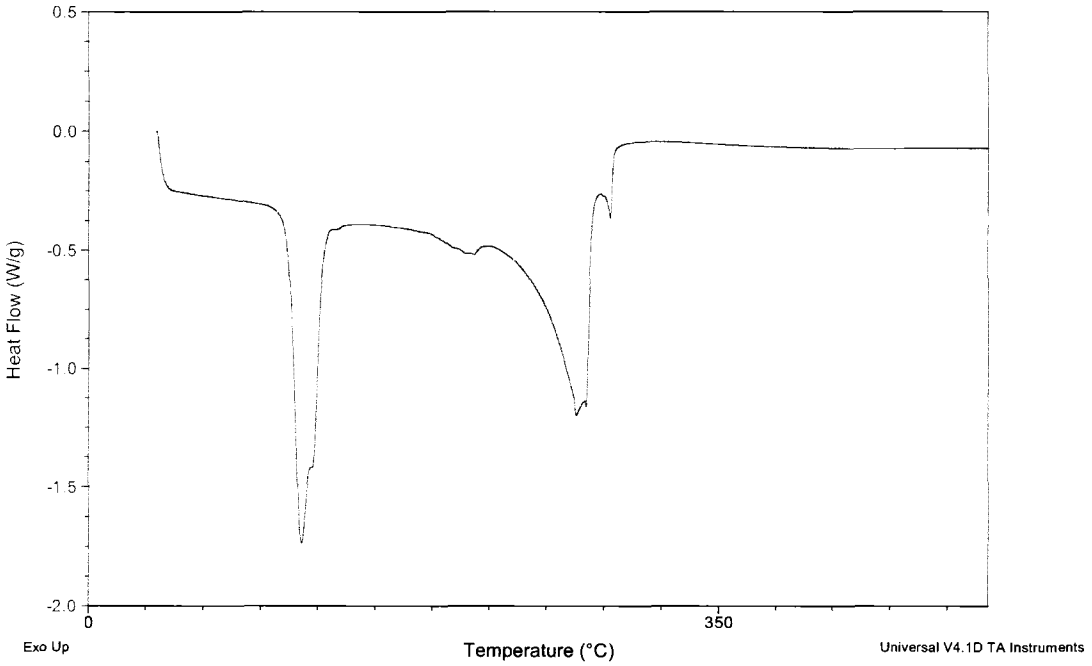

Figure 39: *Differential Scanning Calorimetry Data of Compound 11.*

The TGA of $AlMe_2$(ipip) shows two volatilization events, visible in the derivative weight percent. Due to the small nature of the first volatilization event, it is likely due to the presence of a solvent of crystallization rather than coordinated solvent since it is at a relatively high temperature (120°C). However, the following volatilization curve looks quite clean with a slow onset of volatilization and a quick drop-off as the material is used up. This is followed by a very low residual weight, which is under 10%. The DSC shows one major and one minor endotherm. The first endotherm at 81°C is likely to be the melting point as it is confirmed by bench-top methods where the melting point was found to be 82°C. The second minor endotherm is broad and is therefore likely to be volatilization.

The TGA of Cu(ipip) shows the onset of volatilization (5% weight loss in TG) to be 154°C. The volatilization is clean with a slow onset and a steep drop-off. This is a very clean volatilization curve, which implies the lack of decomposition. However, the onset of volatilization is very high. This may be explained if the compound is a dimer. The DSC shows two endothermic events occurring at 120°C and 270°C. The first event is most likely not melting since there was no melting point at this temperature when using bench-top methods. There was no true bench-top melting point since there was decomposition at 135°C. Since it is likely that this compound is a dimer, perhaps the first endotherm might be due to the splitting of the dimer into monomers, which would have a higher volatility. Another possibility is that it is a rearrangement of the crystal. This may also explain the corresponding small weight loss in the TGA at this temperature, as it could be solvent of crystallization, which is released by the crystal rearrangement. This could be shown to be a reversible crystal rearrangement by doing a DSC from high to low

temperature if it were to show a corresponding exotherm at the same temperature. Because of the low volatility of compound **11**, it would be a difficult compound to use as a precursor in ALD. It could be done, however the process would be fairly slow due to low concentrations of the precursor in the gas phase, and therefore it would take a long time to reach saturation.

4 Conclusions

The insertion of carbodiimides into group 13 metal-amide bonds has been shown to be a facile way to synthesize homoleptic, six-coordinate guanidinato complexes of aluminum and gallium, as well as to make mixed guanidinato-amido compounds for these metals. The compounds are volatile solids and show no thermal decomposition during volatilization, which suggests that they would be valuable precursors for the vapour deposition of group 13-containing thin films. Their synthesis is straightforward, yet there appears to be two mechanisms involved in reaching a final product using stoichiometric control. Initial rapid insertion (several minutes) reactions of carbodiimide into all of the metal-amido bonds leads to the tris(guanidinate) complexes and unreacted starting metal compound. This is then followed by ligand scrambling to produce the stoichiometric product over a time scale of several hours. Subsequent ligand scrambling has been seen in the case of **3** with aluminum trichloride to produce the mixed guanidinato-chloro compound **7**.

All seven complexes were structurally characterized, and compounds **1**, **2**, **4**, **5**, and **7** were shown to exhibit structural features within the chelate rings and for the non-coordinated N centre, which suggests a zwitterionic resonance structure. Compounds **3** and **6** did not exhibit this structural feature. Finally, steric crowding appears to prevent

isopropyl rotation in the guanidinate ligand, and a variable temperature H NMR of **6** showed that this steric locking was circumvented at temperatures above room temperature. These guanidinate complexes show promise as ALD precursors. However, the decomposition route via CDI deinsertion may be problematic in attempting to get ALD growth. Since compounds **1** and **4** avoid this decomposition route, they are the most promising as ALD precursors.

The synthesis for both the aluminum and copper ipip complexes were facile and quick and gave high yields. However, the synthesis for the ligand itself is not as straightforward and it takes a couple of weeks to make enough to be used in one reaction. Greater optimization of the synthesis of ipip is required if this is to become a reasonable alternative to guanidinate-type ligands. The new ipip ligand shows promise as a substitute for guanidinate-type ligands as it avoids this decomposition route. Unfortunately, the ipip complexes formed so far have been dimers, and are therefore less favourable for ALD because of their inherently low volatility.

References

1. Grochowski, E.; Halem, R. D. *IBM Systems Journal*, Vol 42, *338* No. 2, **2003**
2. Ritala, M.; Leskala, M. Handbook of Thin Film Materials Vol. 1: Deposition and Processing of Thin Films, *Academic, San Diego, CA*, **2002.**
3. Mattox, D.M.. Handbook of Physical Vapor Deposition (PVD) Processing. *William Andrew Publishing/Noyes*. **1998**
4. Leskelä, M.; Ritala, M. *Angew. Chem. Int. Ed.* **2003**, *42*, 5548.
5. Ott, A. W.; Klaus, J. W.; Johnson, J. M.; George, S.M. *Thin Solid Films.* **1997,** *292,* 135-144.
6. George, S. M.; Ott, A. W.; Klaus, J. W. *J. Phys. Chem.* **1996,** *100,* 13121-13131.
7. Puurunen, R. L.; Root, A.; Sarv, P.; Viitanen, M.M.; Brongersma, H.H.; Lindblad, M.; Krause, A.O.I. *Chem. Mater.* **2002,** *14,* 720-729.
8. Andre, C. L.; El-Zein, N.; Tran, N.; *Journal of Crystal Growth.* **2007**, *298*, 168.
9. Bailey, P. J.; Bone, S. F.; Mitchell, L. A.; Parsons, S.; Taylor, K. J.; Yellowlees, L. J. *Inorg. Chem.,* **1997,** *36(5),* 867-871.
10. (a) Wood, D.; Yap, G. P. A.; Richeson D. S. *Inorg. Chem.* **1999,** *38,* 5788-5794. (b) Bailey, P. J.; Grant, K. J.; Mitchell, L. A.; Pace, S.; Parkin, A.; Parsons, S. *J. Chem. Soc. Dalton Trans.* **2000,** 1887.
11. (a) Chang, C. C.; Hsiung, C. S.; Su, H. L.; Srinivas, B.; Chiang, M. Y.; Lee, G. H.; Wang, Y. *Organometallics*, **1998,** *17,* 1595. (b) Chang, C. C.; Ameerunisha, M. S. *Coord., Chem. Rev.* **1999,** *189,* 199.
12. Kenney, A. P.; Yap, G. P. A.; Richeson, D. S.; Barry, S. T., *Inorg. Chem.,* **2005,** *44(8),* 2926-2933.
13. Rowley, C. N.; DiLabio, G. A.; Barry, S. T. *Inorg. Chem.* **2005** , *44* , 1983.
14. Zhang, J.; Cai, R.; Weng, L.; Zhou, X. *J. Organometallic Chem.* **2003,** *672,* 94-99.
15. Coles, M. P.; Hitchcock, P. B. *Eur. J. Inorg. Chem.,* **2004,** 2662-2672.
16. Brazeau, A. L.; DiLabio, G. A.; Kreisel, K. A.; Monillas, W.; Yap, G. P. A.; Barry, S. T.; *Dalton Trans.,* **2007**, 30, 3297.
17. Brazeau, A. L.; *M.Sc. Thesis, Carleton University*, **2007.**
18. Bailey, P. J.; Grant, K. J.; Pace, S.; Parsons, S.; Stewart, L. J. J. Chem. Soc., Dalton *Trans.,* **1997,** 4263–4266.
19. Bailey, P. J.; Gould, R. O.; Harmer, C. N.; Pace, S.; Steiner, A.; Wright, D. S. *Chem. Commun.,* **1997,** 1661-1662.
20. Bailey, P. J.; Pace, S. *Coordination Chemistry Reviews,* **2001,** *214,* 91–141.
21. Rodriguez, G.; Sperry, C. K.; Bazan, G. C. *Journal of Molecular Catalysis A: Chemical* **1998**, *128,* 5–28.
22. Bailey, P. J.; Grant, K. J.; Parsons, S. *Organometallics* **1998,** *17,* 551-555.
23. Tin, M. K. T.; Yap, G. P. A.; Richeson, D. S. *Inorg. Chem.* **1998,** *37,* 6728-6730
24. (a) Aeilts, S. L.; Coles, M. P.; Swenson, D. C.; Jordan, R. F. *Organometallics* **1998**, *17*, 3265. (b) Coles, M. P.; Jordan, R. F. *J. Am. Chem. Soc.* **1997,** *119*, 8125. (c) Dagorne, S.; Guzei, I. A.; Coles, M. P.; Jordan, R. F. *J. Am. Chem. Soc.* **2000**, *122*, 274.
25. (a) Meier, R. J.; Koglin, E. *J. Phys. Chem. A* **2001**, *105*, 3867. (b) Barker, J.; Blacker, N. C.; Phillips, P. R.; Alcock, N. W.; Errington,W.; Wallbridge, M. G. H. *J. Chem. Soc., Dalton Trans.* **1996**, 431.

26. Nakamura, S.; Senoh, M.; Nagahama, S.; Iwasa, N.; Yamada, T.; Matsushita, T.; Sugimoto, Y.; Kiyoku, H. *Appl. Phys. Lett.* **1996**, *69*, 4056.

27. For aluminium, see: Waggoner, K. M.; Olmstead, M. M.; Power, P. P. *Polyhedron* **1990**, *9*, 257. For gallium, see: No¨th, H.; Konrad, P. *Z. Naturforsch.* **1975**, *30b*, 681.

28. (a) Mullins, S. M.; Duncan, A. P.; Bergman, R. G.; Arnold, J. *Inorg. Chem.* **2001**, *40*, 6952. (b) Bazinet, P.; Wood, D.; Yap, G. P. A.; Richeson, D. S. *Inorg. Chem.* **2003**, *42*, 6225.

29. Kormos, B. L.; Cramer, C. *J. Inorg. Chem.* 2003, 42, 6691 and references therein.

30. Addison, A. W.; Rao, T. N. *J. Chem. Soc. Dalton Trans.* **1984**, 1349.

31. Pederson, E. B.; *Acta Chem. Scand. B*, **1980**, *34*, 369.